Molybdenum Nanosheet-Functionalized Laser-Induced Graphene with Glycine Oxidase for Electrochemical Sensing of Glyphosate

Rayhane Zribi[a,b†], Zachary T. Johnson[c†], Griffin P. Ellis[c], Christopher J. Banwart[c], Jemima Opare-Addo[d,e], Shelby L. Hooe[f], Joyce C. Breger[f], Antonino Foti[b], Pietro G. Gucciardi[b], Emily A. Smith[d,e], Carmen Gomes[c], Igor L. Medintz[f], Giovanni Neri[a], and Jonathan C. Claussen[c]**

[a] Department of Engineering, University of Messina, C.da Di Dio, I-98166 Messina, Italy
CNR IPCF Istituto per i Processi Chimico-Fisici, viale F. Stagno D'Alcontres 37, I-98156 Messina, Italy

[b] CNR IPCF Istituto per i Processi Chimico-Fisici, viale F. Stagno D'Alcontres 37, I-98156 Messina, Italy

[c] Department of Mechanical Engineering, Iowa State University, Ames, Iowa 50011, United States

[d] Department of Chemistry, Iowa State University, Ames, Iowa 50011, United States

[e]The Ames Laboratory, U.S. Department of Energy, Ames, Iowa 50011, United States

[f] Center for Bio/Molecular Science and Engineering, Code 6900, U.S. Naval Research Laboratory, Washington, D.C., 20375, United States

[*]Author to whom correspondence should be addressed. jcclauss@iastate.edu, gneri@unime.it

[†]Authors contributed equally to this work.

Keywords: electrochemical biosensing, transition metal dichalcogenides, molybdenum disulfide, molybdenum diselenide, laser-induced graphene, glyphosate

Abstract

The widespread use of the pesticide glyphosate has raised concerns regarding its potential health and environmental impacts. Consequently, there is an increasing demand for monitoring glyphosate levels in surface waters and food products. Currently, there is no commercially available rapid, field-deployable sensor capable of quantifying glyphosate concentrations in environmental samples. This study presents the development of a biosensor based on laser-induced graphene (LIG) that is functionalized with transition metal dichalcogenides (TMDs) and the enzyme glycine oxidase. The LIG is created through a scalable process using a CO_2 laser to convert polyimide into a porous, nano/microstructured graphene architecture. The high surface area of LIG acts as a conductive scaffold for subsequent functionalization of both molybdenum disulfide (MoS_2) and molybdenum diselenide ($MoSe_2$) to further improve the electroactive surface area of the electrode. The sensors demonstrate linear sensing ranges from 10-90 μM glyphosate with detection limits of 4.0 and 6.1 μM for LIG electrodes modified with MoS_2 and $MoSe_2$, respectively. Furthermore, the sensors display negligible interference from commonly applied agrochemicals while capable of monitoring glyphosate in food slurries as confirmed with liquid chromatography-mass spectrometry. The developed sensor combines scalable manufacturing with cost-effective TMDs, providing a robust approach for glyphosate assessment in food products.

Introduction

The pesticide glyphosate is the most widely used herbicide across the globe to ensure weed control in both agricultural and residential settings.[1] Glyphosate has recently come under heavy scrutiny due to concerns about its potentially adverse effects on human health.[2] The International Agency for Research on Cancer (IARC) classified glyphosate as a probable human carcinogen, and (aminomethyl)phosphonic acid (AMPA), one of its main metabolites, is strongly associated with genotoxicity and oxidative stress—factors linked to various human diseases, including inflammation, neurodegenerative conditions, cardiovascular diseases, and cancer.[3,4] This criticism has even led one producer to voluntarily cease selling glyphosate for residential use in the United States.[5] Extensive, large-scale use of glyphosate raises the potential for environmental accumulation that poses a chronic health risk to animals and humans exposed to these residues through the water and food they consume.[6,7] To address this concern, there is a growing demand for the development and implementation of low-cost pesticide sensors throughout the food supply chain, ensuring timely detection and mitigation of potential risks to human and animal health.[8] However, current glyphosate detection technology requires field samples be shipped to laboratories for expensive analysis that requires extensive sample preparation as well as highly skilled personnel to analyze the samples. Despite being the most widely applied herbicide, glyphosate is paradoxically one of the most challenging to detect, a phenomenon often referred to as the 'Glyphosate Paradox'.[9]

A plethora of in-field, glyphosate sensor research has valiantly tried to address the 'Glyphosate Paradox.' However, a careful review of the various types of sensors developed underscores their limitations and the necessary enhancements required to create glyphosate sensors suitable for widespread deployment. For example, field-effect transistors (FETs) have been

coupled with Cu^{2+} competitive binding,[10–12] cyanobacteria photosynthetic activity,[13] and CdS/ZnO heterojunctions[14] to detect glyphosate. Nevertheless, FETs can present issues with non-specific binding and adsorption due to their sensitivity to temperature, humidity, and pH, while their complex fabrication often makes them too expensive for widescale environmental monitoring.[15] Some have detected glyphosate using chemiluminescent sensors functionalized with glyphosate oxidase on ZnO with LODs less than 1 μM but utilize complex equipment that is not field deployable and cannot be miniaturized for ease-of-use.[16] Additionally, chemiluminescent sensing in turbid samples may suffer optically and presents analytical and equipment complications associated with fluid addition and monitoring while analyzing samples.[17] Molecularly imprinted polymers (MIPs) have demonstrated remarkable LODs (5 fg/mL to 0.046 μg/mL) but either utilize expensive gold materials or test for limited target species.[18,19] Furthermore, scaling up MIP fabrication presents challenges in manufacturing processes and maintaining compliance with established laboratory protocols.[20] Electrochemical sensors, which generate electronic signals through protein binding and/or the oxidation and reduction of species, offer promising prospects in various sensing domains.[21,22] These devices can be integrated into user-friendly technologies and interfaces for the end user.[23] Typically, electrochemical sensors are made from conductive materials like gold, platinum, or carbon.[24,25] Of the carbon materials, graphene is widely used due to its electrical conductivity, high surface area, low-cost, and electroactive sites.[26] Furthermore, we contend that the utility of laser-induced graphene (LIG) holds key advantages over other carbon-based sensors due to its ease-of-fabrication, elimination of post-print annealing, and avoidance of ink synthesis and volatile solvents. Additionally, the high surface area of these LIG electrodes is particularly well suited for subsequent functionalization with nanomaterials, such as noble metal nanoparticles and enzymes, to improve the efficiency of superficial redox reactions

and to assist in selectively monitoring pesticides.[27] Our research group, along with others, has employed enzyme functionalized LIG for electrochemical pesticide monitoring, encompassing organophosphate insecticides,[28,29] fungicides,[30] and even the herbicide glyphosate.[31] In each instance, the LIG was enhanced with gold or platinum nanoparticles to boost its catalytic properties, thus improving the sensor's sensitivity for on-site pesticide detection, albeit at an increased initial manufacturing cost.

To improve the performance of electrochemical sensors and to reduce the reliance on costly noble metals in electrochemical electrodes, researchers have recently turned to 2D molybdenum-based nanosheets to enhance electrochemical reactivity.[32,33] Molybdenum-based nanosheets have attracted rapidly growing interest for their unique properties and 2D structures, which have demonstrated potential in sensing applications by enhancing the sensitivity and selectivity of sensors towards specific targets.[34–36] Recently, 2D transition metal dichalcogenides based on sulfides and selenides have become the most used materials for biosensors.[34] Molybdenum disulfide (MoS_2), as well as molybdenum diselenide ($MoSe_2$), have become potential biosensor component candidates due to their promising electrocatalytic properties. MoS_2 and $MoSe_2$ are semiconductors possessing an indirect bandgap transition energy, which turns to direct going from bulk to monolayers, enabling fast charge transfer to boost sensing performance.[37] In addition to this, these bidimensional materials offer high-carrier mobility and a large surface-to-volume ratio depending upon how they are implemented.[38] Specific to electrochemical sensing, electrodes fabricated with MoS_2 or $MoSe_2$ detect at lower and negative potentials than those fabricated with noble metals like platinum, which reduces the risk of interference from species like chlorine and nitrite, thereby enhancing specificity and reliability in complex food and agricultural samples.[39–41] To harness the benefits of both carbon materials and molybdenum nanomaterials, researchers

have combined these materials and explored the electrocatalytic properties of various MoX_2-graphene heterogeneous structures. Different methods have been explored to pair the electrocatalytic properties of both materials using mixed-dimensional heterostructures for photodetectors,[42] lateral grown heterostructures through band alignment engineering,[43] and nanocomposites for improved lithium-ion battery storage.[44] Additionally, researchers have found that the combined MoS_2 and graphene heterostructures reduced the work function compared to graphene alone.[45] Furthermore, it has been shown that increasing the layers of MoS_2-graphene heterostructures can directly improve and tune the charge transfer capabilities of the overall material.[46] To further demonstrate the utility of MoS_2-graphene heterostructures, researchers have created an NO_2 gas sensor owing its advantages to the exposed active edge sites of the MoS_2-graphene heterostructures.[47] Others have utilized MoS_2-graphene heterostructures in electrochemical sensing applications for pathogens,[48] flavonoids,[49] and even the organophosphate pesticide methyl parathion.[50] However, to our knowledge, MoS_2/$MoSe_2$-graphene heterostructures have not been previously demonstrated for electrochemical glyphosate monitoring.

In this work, we investigate the use of 2D-MoS_2 and 2D-$MoSe_2$ nanosheets produced via liquid phase exfoliation (LPE) and liquid cascade centrifugation (LCC)[51–53] in improving the sensing performance of an enzymatic glyphosate electrochemical sensor by taking advantage of the enhanced electroactive surface area of the monodispersed Mo-based nanosheets on an LIG platform. We demonstrate the fabrication of MoX_2-LIG heterostructures and their utility for electrochemical sensing, offering a useful and cost-effective sensing platform that does not require expensive metallic nanoparticles like gold, platinum, or silver with the added benefits of the biocompatibility associated with MoS_2 and notable electro-conductive properties of $MoSe_2$.[54] Notably we introduce several important concepts for electrochemical detection of the herbicide

glyphosate with an electrode functionalized with glycine oxidase: (1) MoS_2 and $MoSe_2$ permit the operation of the electrode at a negative working potential (i.e., -0.15 V *vs* Ag/AgCl) which reduces or eliminates the interference of electroactive species found endogenously in field samples, (2) differential pulse voltammetry can be used to monitor the glyphosate-glycine oxidase reaction on the electrode surface which enhances signal-to-noise ratios of the sensor and improves target detection in complex mixtures , and (3) noble metals can be completely eliminated from the sensor design. Consequently, the resultant MoX_2-LIG electrochemical sensors exhibited glyphosate limits of detection (LOD) of 4.0 and 6.1 μM for LIG electrodes functionalized with MoS_2 and $MoSe_2$, respectively. This performance underscores the suitability of the sensors for food safety analysis, particularly given that glyphosate concentrations in soybeans and pinto beans range from 3 to 10 μM.[55] Furthermore, the sensors demonstrated consistent monitoring of glyphosate in actual soybean and canned pinto bean samples as confirmed with liquid chromatography coupled with mass spectrometry (LC-MS), yielding recovery percentages ranging from of 81.3% to 120%.

Results & Discussion

1. Sensor Fabrication

The fabrication and functionalization process for the developed 3-electrode enzymatic MoX_2-LIG biosensor is illustrated in **Figure 1**. The conductive base layer of the sensors, consisting of LIG, was created by irradiating polyimide film with a commercial CO_2 laser. This process transformed sp^3 carbons in the polyimide film into sp^2 hybridized carbons.[56] Next, Ag/AgCl ink was painted onto the reference LIG electrode and coated with a salt-loaded PVC membrane to establish a stable and durable solid-contact pseudo-reference for the biosensor.[57] To improve the electroactive surface area properties of the working electrode, the respective MoX_2 nanomaterials,

centrifuged at 1.5 krpm, were progressively drop-coated onto the surface of the working electrode until the desired volume was deposited. Concurrently, the surface was heated to 100 ºC to decrease the drying time of the MoX_2 coatings. See the Methods and Materials section for MoX_2 suspension preparation and electrode optimization by varying the centrifugation rate and drop-coated volume. The MoX_2 modified LIG working electrodes were then biofunctionalized with the glyphosate biorecognition agent glycine oxidase, glutaraldehyde as the cross-linker, and flavin adenine dinucleotide (FAD) as the cofactor, similar to our previous work.[31] The electrochemical detection of glyphosate and a simplified chemical reaction are illustrated in **Figure 1e**. Scheme 1 demonstrates the enzymatic reaction and sensing mechanism between the enzyme glycine oxidase and its substrate, glyphosate, facilitated by the developed biosensor.[58] To further underscore the cost-effectiveness of the fully functionalized sensor, a materials cost analysis was conducted, as detailed in **Table S1**, revealing a cost of $14.55 per sensor. The enzyme glycine oxidase represented the majority of this cost at approximately $14.42 per sensor. Consequently, sourcing a vendor capable of scaling up enzyme production could significantly reduce the overall materials costs of the sensor.

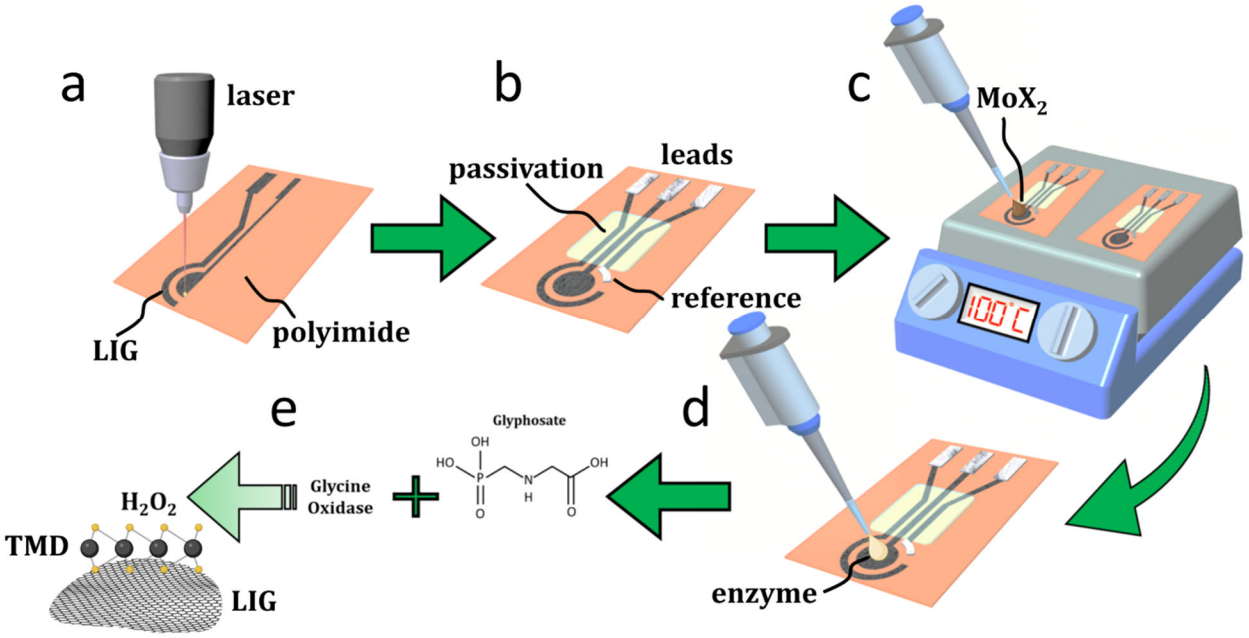

Figure 1. Sensor fabrication and functionalization schematic. a) Laser irradiation of polyimide film into amorphous graphene, b) application of silver electrical leads, acrylic passivation layer, and a silver/silver chloride reference to the LIG 3-electrode design, c) MX_2 drop-coating onto the LIG working electrode while heated at 100 ºC, d) enzymatic functionalization of working electrode, e) simplified enzymatic reaction scheme resulting in the product, H_2O_2, which is subsequently reduced at the MoX_2-LIG working electrode.

Scheme 1. Reaction scheme of glyphosate with glycine oxidase (GlyOx) with (aminomethyl)phosphonic acid (AMPA) as the primary degradation product of glyphosate. Scheme also shows the reduction of hydrogen peroxide (H_2O_2) at the developed biosensor surface.

$$\mathrm{GlyOx - FAD_{ox} + glyphosate \Longrightarrow GlyOx - FAD_{red} + AMPA + glyoxylate}$$

$$\mathrm{GlyOx - FAD_{red} + O_2 \Longrightarrow GlyOx - FAD_{ox} + H_2O_2}$$

$$\mathrm{H_2O_2 + 2e^- \Longrightarrow 2OH^-}$$

2. Materials Characterization

As outlined in Scheme 1, hydrogen peroxide (H_2O_2) is produced during the enzymatic reaction, and various Mo-based nanomaterials have been investigated for its detection, with studies utilizing MoS_2 and $MoSe_2$ surfaces to measure H_2O_2 in contexts ranging from intracellular spaces to tumor cell byproducts and biological fluids such as urine and serum.[59–62] For this reason, 2D-MoS_2 and

2D-$MoSe_2$ were selected as candidates to modify the LIG surface and, thus, develop a new avenue for glyphosate detection.

To gain a deeper insight into the morphologies and compositional properties of the MoX_2 and laser-induced graphene (LIG) electrode materials, we utilized a suite of characterization techniques. These included scanning electron microscopy (SEM) for detailed imaging of surface morphology, dynamic light scattering (DLS) for assessing particle size distribution, and energy dispersive X-ray (EDX) analysis for elemental composition determination (**Figure 2**). SEM images revealed the morphology and nanostructures, visually confirming the successful exfoliation and deposition of nanomaterials on the LIG surface and showed the heterogeneous MoX_2-LIG composition (**Figure 2a-b,d-e**). Cross-section images (**Figure S1**) indicated an average LIG thickness of 31.4 ± 3.2 μm. DLS analysis clarified the size distribution of nanoparticles in the MoS_2 colloidal dispersion, revealing a range from 231 nm to 5.3 μm, with the relative intensities of the respective sizes being 98.2% and 1.8% (**Figure 2c**). For the $MoSe_2$ colloidal dispersion, a narrow distribution peak near 100.6 nm was observed (**Figure 2f**). The low polydispersity indexes of 0.274 for MoS_2 and 0.249 for $MoSe_2$ suggested highly monodisperse suspensions, a finding in agreement with the SEM observations. It should be noted here that previous studies have characterized MoS_2 and $MoSe_2$ materials, observing a wide variety of particle sizes and distributions. Notably, a nanocomposite for drug delivery, incorporating MoS_2 with starch and chitosan, was synthesized through hydrothermal treatment.[63] This method achieved a comparable polydispersity index (PDI) of 0.2; however, it required an extensive and intricate synthesis process that involved high temperatures, pressures, and multiple solvents. Liquid phase exfoliation (LPE) of 2D materials like MoS_2 and $MoSe_2$ offers simplicity and cost efficiency compared to other methods, including the hydrothermal approach previously mentioned.

Nonetheless, LPE faces inherent challenges, such as wide size distributions and relatively large lateral dimensions.[64] However, LPE coupled with liquid cascade centrifugation (LCC), the technique used in this research, has boasted fine control and high yield of nanosheet dispersions and uniform size distributions, thus explaining our monodispersed suspensions for both materials.[65] Moreover, EDX of the MoS_2 and $MoSe_2$ nanosheets based-LIG confirmed the presence and the well distribution of the main Mo, S, and Se elements on the electrode surface (**Figure 2g-l**). The EDX spectra is shown in **Figure S2**, which indicated no contaminants.

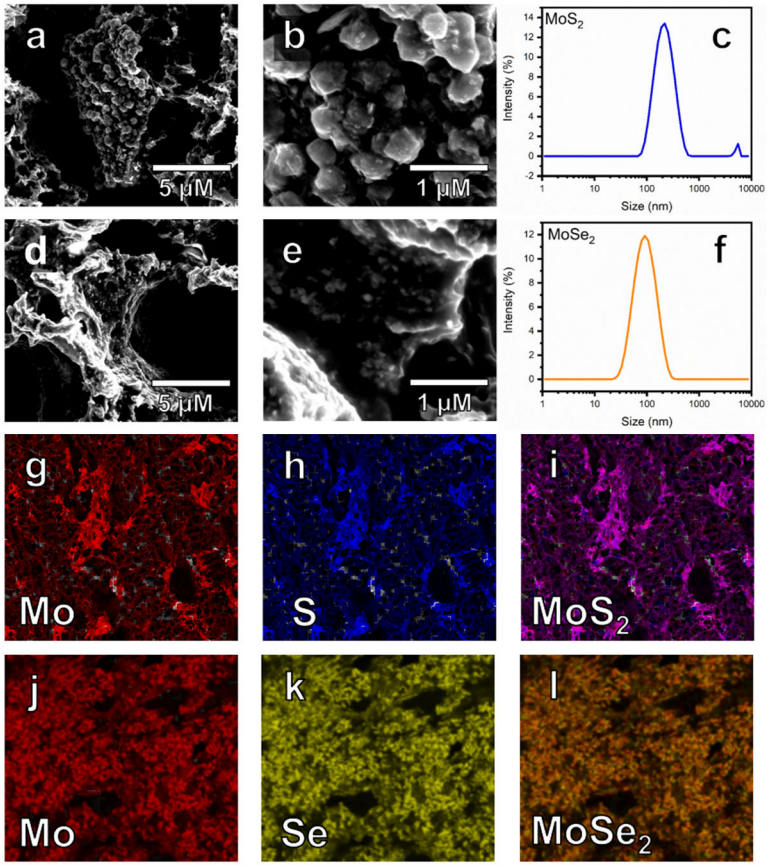

Figure 2. Morphology and size characterization portraying a-b) SEMs of LIG-MoS_2 heterostructures at 5,000X and 25,000X, c) DLS size distribution of the MoS_2 liquid suspension, d-e) SEMs of LIG-$MoSe_2$ heterostructures at 5,000X and 25,000X, f) DLS size distribution of the $MoSe_2$ liquid suspension, EDX mapping of LIG-MoS_2 for g) Mo, h) S, i) combined MoS_2, and EDX mapping of LIG-$MoSe_2$ for j) Mo, k) Se, and l) combined $MoSe_2$.

To further inspect the material properties of the MoX_2-LIG surfaces, Raman spectroscopy and x-ray photoelectron spectroscopy (XPS) were performed to investigate the chemical makeup

of the modified surfaces (**Figure 3**). The Raman spectrum (**Figure 3a-b**), which was collected using an excitation wavelength of 532 nm, identified the characteristic E^1_{2g} (383 cm^{-1}) and A_{1g} (408 cm^{-1}) peaks for MoS_2, which correspond to in-plane (E^1_{2g}) and out-of-plane (A_{1g}) vibrational modes within the MoS_2 layer and were consistent with other Raman spectra.[38,51,66–68] MoS_2-modified sensors displaying similar Raman spectra have been developed to detect various biomarkers, such as xanthine and dopamine, but these nanomaterials were synthesized using hydrothermal processes notably more complex than the LPE-LCC process used in this work; thus, this characterization highlights the inherent benefits of LPE-LCC compared to hydrothermal methods while yielding similar material properties.[69,70] Additionally, the sole and distinctive A_{1g} (242 cm^{-1}) peak was observed for the $MoSe_2$ sample, indicating a 2H-$MoSe_2$ structure.[71] Previous research has developed $MoSe_2$ and graphene hybrids for sodium storage, utilizing either Hummer's method or hydrothermal processes to produce graphene, which adds complexity compared to the simpler laser conversion process employed in this study.[72,73] Characteristic graphene peaks were assigned to the D (1350 cm^{-1}), G (1580 cm^{-1}), and 2D (2690 cm^{-1}) bands where the D band corresponds to defects in the graphene, G band indicates in-plane vibrations, and 2D band represents second order zone-boundary phonons.[74] The intensity ratio between the D and G peak, I_D/I_G, was calculated to be 1.1 and suggested a defect-rich surface. The intensity ratio between the 2D and G peak, I_{2D}/I_G, corresponds to the number of graphene layers and was found to be 0.4, indicating multilayered graphene ($I_{2D}/I_G < 1$).[75] XPS measurements displayed various peaks which were identified as the carbon (C 1s), oxygen (O 1s), molybdenum (Mo 3p, Mo 3d), sulfur (S 2s, S 2p), and selenium (Se 3s, Se 2p, Se 3d) components similar to other MoX_2-graphene heterostructure reports (**Figure 3c-f**).[71,76,77] Residual sodium from the surfactant used to stabilize the suspensions was observed at the Na 1s band (1067.7 eV). The O 1s band (532.0 eV) indicated

the oxygen functionality of the surface necessary for enzyme attachment while the C 1s peak (281.0 eV) contained sp2-hybridized carbons. The high-resolution Mo 3d band (**Figure 3d**) contained three common peak locations in both the MoS_2 and $MoSe_2$ samples namely the $3d_{5/2}$ (~229 eV) and $3d_{3/2}$ (~232 eV) peaks resultant of the Mo (IV) oxidation state as well as a strong peak near 235.2 eV opined to be the Mo (VI) species represented by the Mo-O-C bond.[71,78] Additional peaks were observed to be shifted from the $3d_{5/2}$ and $3d_{3/2}$ bands, signifying both 2H and 1T structures were present.[79] The deconvoluted S 2p spectrum (**Figure 3e**) possessed the $2p_{3/2}$ and $2p_{1/2}$ orbitals consistent with other works.[80] The Se 3d spectrum (**Figure 3f**) displayed the characteristic $3d_{5/2}$ and $3d_{3/2}$ with smaller and slightly shifted peaks believed to indicate a mix of 2H and 1T structures as mentioned previously.[81,82]

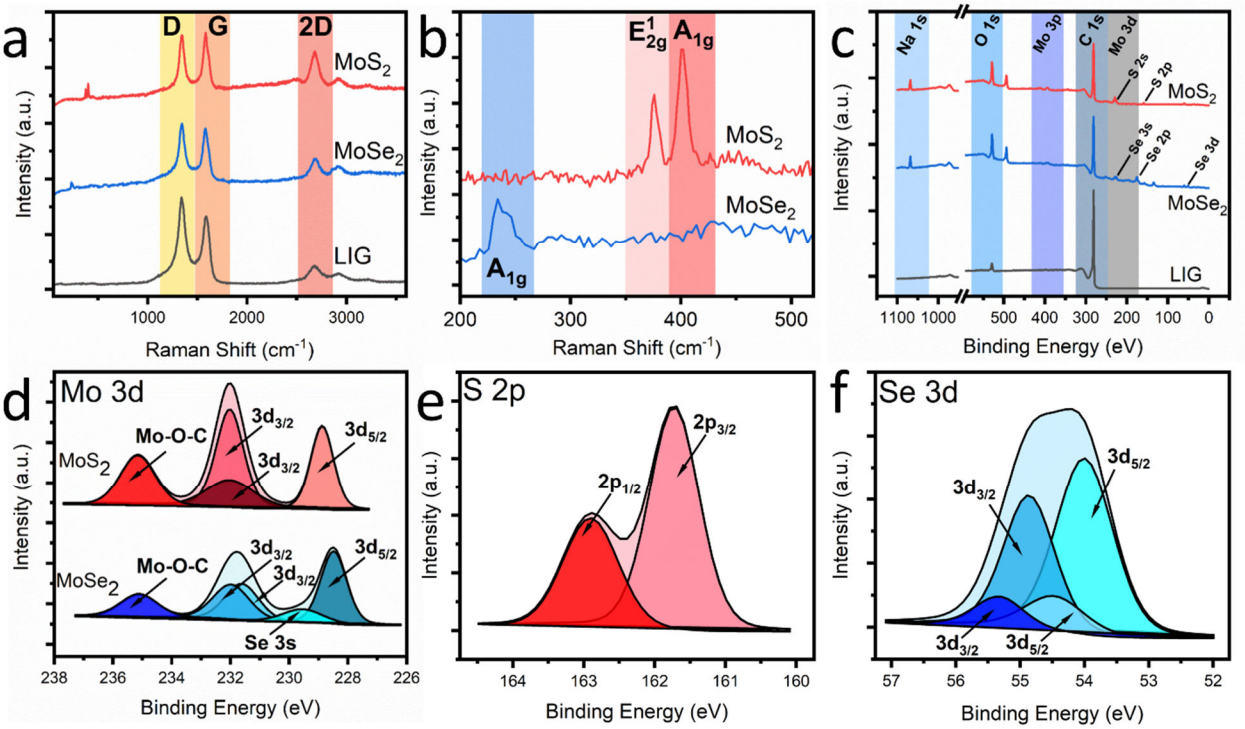

Figure 3. Material composition characterization portraying a) Raman spectrum of LIG-MoS_2 (red), LIG-$MoSe_2$ (blue), and LIG (black), b) zoomed-in Raman of MoS_2/$MoSe_2$ modes, c) XPS survey, d) deconvoluted Mo 3d band, e) deconvoluted S 2p band, and f) deconvoluted Se 3d band.

3. Electrochemical Characterization

The electrochemical characterization of MoX_2-LIG sensors and the verification of nanomaterial and enzyme functionalization were both conducted through cyclic voltammetry (CV) in a solution containing the redox probe ferri/ferrocyanide (**Figure 4a,d**). The electrode and cable connections are shown in **Figure S3**. As MoX_2 nanomaterial was deposited onto the LIG surface, an increase in the anodic and cathodic currents were observed, indicating an increase in the electroactive surface area of the electrode surface due to the MoX_2-LIG heterostructures. Furthermore, after the enzyme functionalization, a decrease in current was observed, indicating successful enzyme attachment, which has been demonstrated in other enzyme-attachment studies using electrochemical impedance spectroscopy on pencil graphite sensors for the detection of glyphosate.[83] Furthermore, cyclic voltammograms obtained at varying scan rates (**Figure 4b,e**) were used to estimate the electroactive surface area (ESA) of the electrodes as well as to produce the corresponding Randles-Sevcik plots (**Figure 4c,f**). These ESA values were calculated using the Randles-Sevcik equation for quasi-reversible systems (**Eq. 1**) where i_p is the cathodic/anodic peak current, A is the ESA, D is the diffusivity, n is the number of electrons transferred in the ferri/ferrocyanide probe, v is the scan rate, and C is the concentration of the redox species.[84] Though linearity was observed in the Randles-Sevcik plots, which typically indicates diffusion-controlled processes, the drift in peak-to-peak potentials as the scan rates increased suggest a quasi-reversible system.[84,85]

$$i_p = 2.63 \times 10^5 \, A \, D^{1/2} \, n^{3/2} \, v^{1/2} \, C \qquad \text{Equation (1)}$$

The MoS_2 and $MoSe_2$ sensors exhibited an ESA of 0.161 cm^2 and 0.178 cm^2, respectively, which constitute 227% and 244% of their respective geometric surface areas. These values surpass the calculated bare LIG ESA of 189%, highlighting the enhanced surface area and distinctive

properties of these nanomaterials on LIG. These ESA values are also consistent with the surface morphology depicted in **Figure 2**, which illustrates the nanomaterial coverage on the LIG and its porous structure. Similar ESA values were previously reported for LIG functionalized with electro- and electroless deposited platinum nanoparticles on identically sized electrodes (3 mm diameter) with values of 0.193 cm^2 and 0.169 cm^2 [31,86]. This evidence suggests that MoS_2 and $MoSe_2$ can offer comparable electroactive surface areas to noble metals such as platinum but with the advantage of reduced cost.

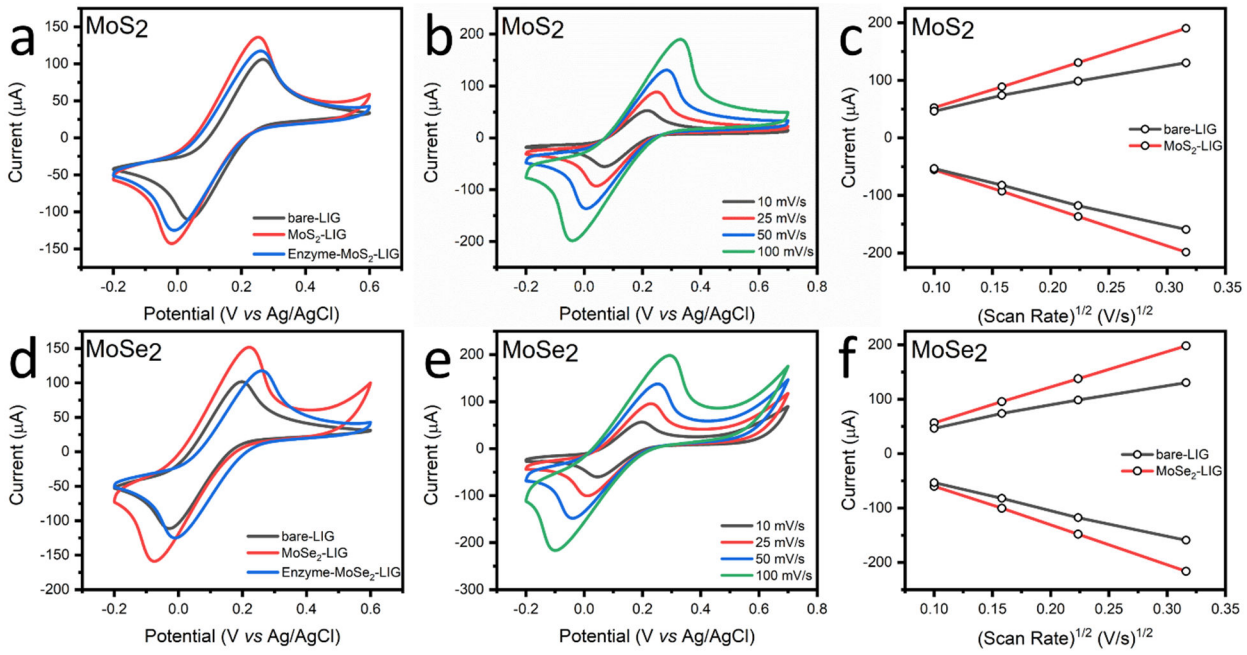

Figure 4. Electrochemical characterization of the MoX_2-LIG sensor. a,d) Cyclic voltammograms in ferri/ferro cyanide at each functionalization step including MoX_2 and enzyme deposition, b,e) cyclic voltammograms in ferri/ferro cyanide at varying scan rates, and c,f) corresponding Randles-Sevcik plots.

4. Enzyme Cross-Linking Study

The developed MoX_2-LIG sensors employ glutaraldehyde (GA) for the immobilization of enzymes, specifically utilizing GA for the covalent attachment of glycine oxidase. This method significantly enhances the long-term stability of the sensors and increases selectivity by reducing non-specific adsorption of interfering compounds found endogenously in solutions.[87] To

determine the most effective glutaraldehyde (GA) concentration for improving biosensor performance, working electrodes were drop-coated with various GA concentrations (0.25%, 0.1%, and 0.01%), along with glycine oxidase and Flavin Adenine Dinucleotide (FAD) (see Experimental Section). These sensors were evaluated against those functionalized with enzymes through covalent bonding using ethyl-3-(3-dimethylaminopropyl) carbodiimide/N-hydroxysuccinimide (EDC/NHS) chemistry. All of these sensor biofunctionalization protocols were designed to observe changes in the glyphosate reduction signal within the 0 to -0.2 V range versus Ag/AgCl, as depicted in **Figure 5a-b**. However, the use of EDC/NHS for linking resulted in a minimal reduction signal when exposed to 1- and 5-mM concentrations of glyphosate. Interestingly, the reduction peak became more pronounced as the concentration of glutaraldehyde was reduced from 0.25% to 0.1%. This suggests that lower concentrations of glutaraldehyde lessen its capacity for cross-linking between enzymes, thereby preserving more enzymatic sites for interaction with glyphosate. Conversely, higher concentrations of glutaraldehyde create more stable and robust covalent bonds, leading to an excess of covalent linkages that may inadvertently diminish enzyme activity.[88] For the MoS_2 sensor, there was a noticeable decrease in the reduction peak when the glutaraldehyde (GA) concentration was lowered from 0.1% to 0.01%, suggesting that such a low concentration was inadequate for effectively attaching the enzyme to the surface of the electrode. Conversely, the $MoSe_2$ sensor demonstrated similar responses at both 0.1% and 0.25% GA concentrations. As a result, a 0.1% concentration of glutaraldehyde (GA) was determined to be the most effective for attaching the enzyme to the surfaces of MoX_2-LIG electrodes, thereby creating the MoX_2-LIG biosensors.

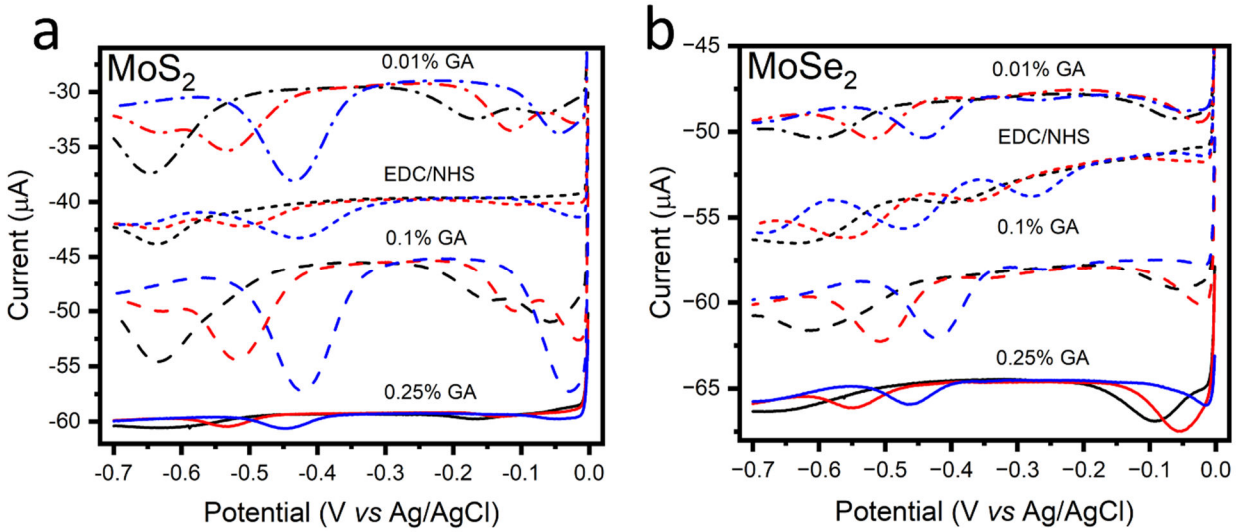

Figure 5. Cross-linking study displaying differential pulse voltammograms for a) MoS_2-LIG and b) $MoSe_2$-LIG electrodes in 10X PBS (black), 1 mM glyphosate (red), and 5 mM glyphosate (blue) at decreasing concentrations of glutaraldehyde and using EDC/NHS chemistry.

5. Glyphosate Detection

The resultant MoX_2-LIG biosensors were calibrated with increasing concentrations of glyphosate (10-90 μM), aligning with the known ranges of glyphosate residues found in food, as shown in **Figure 6a,d**. Differential pulse voltammetry (DPV) was performed in 10X phosphate buffer saline (PBS) pH 7.4 over the reduction range of interest. DPV was selected for electrochemical analysis as this technique limits capacitive noise and produces defined peaks that are characteristic of the target even in the presence of other electroactive species.[89] Distinct reduction peaks were observed near -0.15 V *vs* Ag/AgCl, indicating the successful enzymatic oxidation of glyphosate and by extension, the reduction of hydrogen peroxide at the MoX_2 surfaces. As the concentration of glyphosate increased, the magnitude of the reduction peaks increased as well, indicating linear behavior and good correlation, with an R^2 of 0.961 and 0.987 for the MoS_2-LIG and $MoSe_2$-LIG biosensors, respectively. The corresponding sensitivity plots (**Figure 6b,e**) yielded sensitivities of 47.0 and 22.8 nA/μM and limits of detection (LODs) of 4.0 and 6.1 μM for the MoS_2-LIG and $MoSe_2$-LIG biosensors, respectively. The electroanalytical

performances of the proposed MoX_2-LIG biosensors were compared with those of other glyphosate electrochemical sensors reported in the literature (**Table S2**). Though other works displayed lower LODs (nM to μM), our LOD and linear range effectively address the target concentrations of glyphosate in food extracts. The performances of our sensors are comparable to previously reported state-of-the-art glyphosate electrochemical sensors, with the advantage of using an easy synthesis procedure, simple sensor fabrication, and a sensor capable of detecting glyphosate in the food matrix without employing a complex extraction procedure. Furthermore, our glycine oxidase-based biosensors presented similar LODs and linear ranges compared to other works[31,90,91] that have developed glycine oxidase-based biosensors, which demonstrates that these biosensors have approached their sensing limits as the same enzyme yields similar behavior and figures of merit based upon its enzyme kinetics. Our obtained sensor reproducibility for n=4 sensors of both materials is illustrated in **Figure 6c,f**. The MoS_2- and $MoSe_2$-LIG biosensors performed consistently with average relative standard errors of 5.7% and 12.9%, respectively, thus highlighting the biosensor-to-biosensor reproducibility and reliability. The biosensor repeatability was investigated for n=3 and indicated a strong correlation with an R^2 of 0.977 and 0.996 for MoS_2- and $MoSe_2$-LIG, respectively (**Figure S4**). The sensors were further validated against a control experiment to confirm that the MoX_2-LIG materials without enzyme do not directly engage with glyphosate (**Figure S5**). From this investigation, the DPV comparisons distinctly prove that the MoX_2-LIG materials without enzyme yielded negligible responses compared to the expected signal of the enzymatic sensors. Therefore, it is the sole reaction between glyphosate and glycine oxidase that produces the H_2O_2, which is read electrochemically. Sensor stability over multiple scans was also performed and confirmed accurate readings of 50 μM glyphosate where the signal was maintained at ~90% by the third scan for both electrodes and dropped to 84.2% and 81.3% of

the original signal by the fifth scan for MoS_2- and $MoSe_2$-LIG, respectively (**Figure S6**). The decrease in signal could possibly be attributed to the build-up of byproduct after each scan (AMPA and glyoxylate), which creates a growing diffusion layer that hinders the mass transport of the fresh electroactive byproduct.[92] These results indicated the stable reading of a known concentration of glyphosate can be achieved over multiple scans and suggested that the devices should not be used beyond the third scan without cleaning and refreshing the sensing surface. Furthermore, experiments were conducted at room temperature. As the intended food application requires a homogenization step (see Methods and Materials) that would be performed in a temperature-controlled environment, temperature fluctuations would not be expected.

The sensing mechanism used in this work presents inherent benefits and elucidates many challenges when developing a biosensor with specificity toward the target. The usage of MoS_2 and $MoSe_2$ in the direct reduction of H_2O_2 at negative potentials near -0.15 V *vs* Ag/AgCl demonstrates a key advantage compared to other nanomaterials, such as platinum, that oxidize H_2O_2 at more positive potentials ranging from 0.6 to 0.8 V *vs* Ag/AgCl.[31,90,93] By operating at lower and negative potentials, the likelihood of oxidizing possible interferent species present in food and agricultural samples, including chlorine (1.2 V *vs* Ag/AgCl) and nitrite (0.5 to 1 V *vs* Ag/AgCl), is mitigated.[39–41] Therefore, the MoS_2 and $MoSe_2$ functionalized biosensors avoid a host of interferent species based upon the electrochemical reduction mechanism alone compared to the current literature.

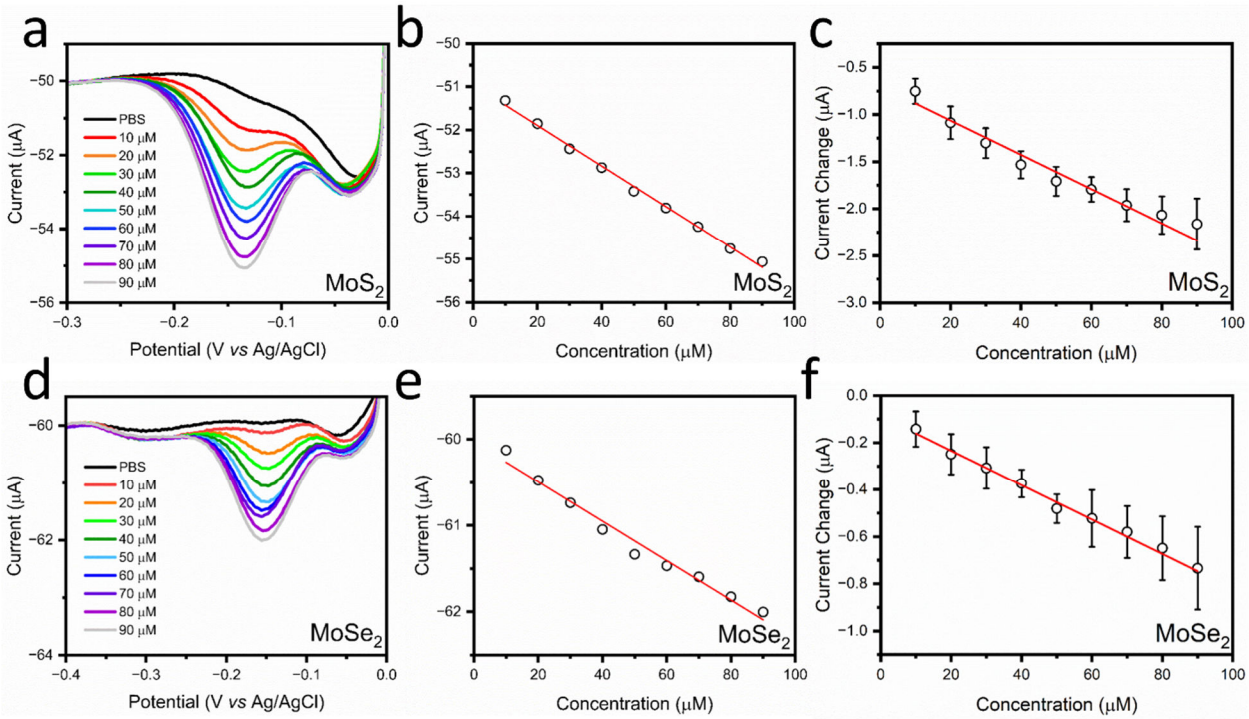

Figure 6. Electrochemical detection of glyphosate with MoS_2-(a-c) and $MoSe_2$-(d-f) modified biosensors. a,d) Calibration of MoX_2-LIG biosensors to increasing concentrations of glyphosate in 10X PBS pH 7.4, b,e) corresponding sensitivity plots displaying the linear range of each biosensor, and c,f) sensitivity plots for n=4 different biosensors.

6. Long-term Stability and Interference

Long-term stability of the MoX_2-LIG biosensors was monitored by performing DPV calibrations over a period of 21-34 days (**Figure S7**). Throughout this duration, the biosensors consistently detected glyphosate, exhibiting average sensitivities of 11 ± 3 and 18 ± 2 nA/µM for the MoS_2-LIG and $MoSe_2$-LIG sensors, respectively. In summary, both types of biosensors demonstrated significant and sustained responses to glyphosate, effectively maintaining the catalytic properties of the MoX_2 materials and stability of the enzyme attachment. We hypothesize that the notable long-term stability of these biosensors can be linked to the pre-calibration conditioning steps. Prior to calibration, each sensor was exposed to glyphosate concentrations of 1 mM and 5 mM—levels significantly higher than those typically encountered in their application.

This pre-exposure is thought to condition the enzyme, maintaining it in an optimal conformation for effective substrate interaction. Such a conditioning process likely contributes to the biosensors maintaining their sensitivity for a period of 21-34 days post-initial calibration. This theory is bolstered by the understanding that protein interactions with external matrices can enhance stability by limiting the protein's structural flexibility, thereby minimizing its likelihood of denaturation.[94] As such, the findings from this long-term stability study underscore the reusability of the biosensors. Additionally, various cross-linking approaches could be investigated to further improve the shelf-life of the electrodes (i.e., comparing stability and sensitivity as a function of the free and bound enzyme amines) by carefully manipulating the covalent linkages between the electrode surface and enzyme.[95]

To further validate the specificity of the biosensors, the developed MoS_2-LIG biosensor underwent testing against various pesticides and (aminomethyl)phosphonic acid (AMPA), a primary degradation product of glyphosate. DPV scans (**Figure S8**) were conducted in environments containing 50 μM glyphosate alongside 50 μM of potential interfering substances, as depicted in **Figure 7**. The selection of interfering pesticides for this analysis was informed by their common presence in similar agricultural products. For example, neonicotinoids are typically applied as seed treatments and may persist in a variety of foods,[96] while the major herbicide, dicamba, is similarly found in foods such as tomatoes.[97] The commonly applied insecticide parathion as well as the fungicide carbendazim were investigated as both persist in food. Trace minerals, such as iron and zinc, were further tested. These experiments were designed to closely mimic real-world conditions, thereby validating the applicability and reliability of the biosensors in detecting glyphosate in complex matrices. Consequently, the acquired signals to glyphosate in the presence of possible interferents yielded recovery signals with respect to the expected signal

to 50 µM glyphosate that ranged from 86.3-111.1% for MoS_2-LIG and 79.3-98.8% for $MoSe_2$-LIG. This data suggests that possible electroactive species do not electrochemically react within the sensing window, and other agrochemicals minimally affect the sensing response to glyphosate with the exception of dicamba on the functionalized $MoSe_2$-LIG device, which produced a recovery percentage of 79.3%. Since the experiment performed with MoS_2-LIG and dicamba produced a recovery percentage of 92.0%, we hypothesize that dicamba did not interfere with the enzyme but interacted with $MoSe_2$ itself by impeding its ability to turnover H_2O_2 possibly due to the functional groups or elements present in dicamba. Therefore, there is an advantage in developing the two similar MoX_2-LIG biosensors, which further elucidates the tradeoffs between MoS_2 and $MoSe_2$ in sensitivity, LOD's, and possible interferent species. It is in comparing the performances of the MoS_2/$MoSe_2$-LIG electrodes that analytical issues can be circumvented with respect to interferent species by using one device over the other.

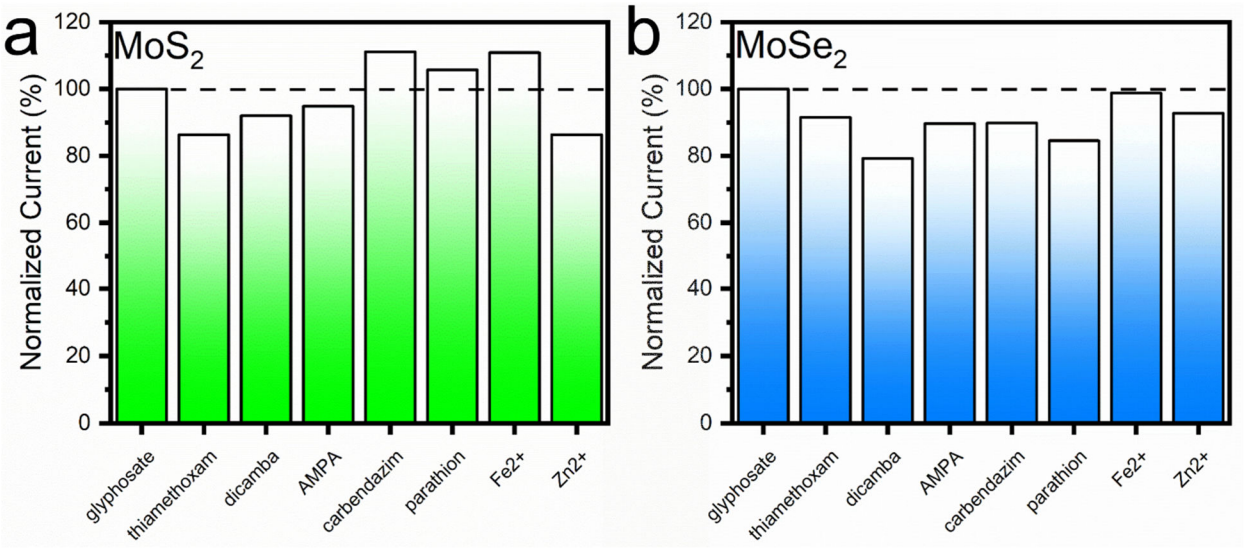

Figure 7. Interference study comparing biosensor responses to 50 µM glyphosate in the presence of 50 µM potential interfering species for a) MoS_2-LIG and b) $MoSe_2$-LIG.

7. Glyphosate Determination in Food Samples

To validate the MoX_2-LIG biosensors, food samples known for high glyphosate residue levels were chosen for testing. Specifically, soybeans and pinto beans, which typically contain glyphosate concentrations ranging from 3 to 10 μM, were selected as ideal candidates for these validation experiments.[55] The glyphosate concentrations in these food samples were quantified electrochemically and confirmed with liquid chromatography-mass spectroscopy (LC-MS). In short, a 1:1 (w/v) slurry of homogenized food sample and 10X PBS were prepared for electrochemical tests (see Experimental Section). Sensors were submerged in this mixture and DPV scans were performed. For (LC-MS) confirmation, the Quick Polar Pesticide (QuPPe) method was used to quickly extract glyphosate from the same homogenized sample.[98] An internal standard (glyphosate-2-^{13}C) was used to improve the accuracy of the LC-MS data. **Figure S9** displays the extracted chromatograms of the calibrated model of glyphosate and the internal standard. **Figure S10** displays the extracted chromatograms of the food samples at a molecular weight of 168.0067 g/mol with a distinguished peak near 1.2 minutes; the linear regression and calibration are shown in **Figure S11**. **Table 1** reports the electrochemical and LC-MS responses with recovery percentages ranging from 81.3 to 120%. The $MoSe_2$-LIG sensors tended to overpredict the presence of glyphosate, suggesting a potential for nonspecific interactions with other components within the food matrices. To address this, a modeling factor was introduced to refine the accuracy of each biosensor readings across different foods, given that both MoS_2- and $MoSe_2$-LIG biosensors reported comparable glyphosate concentrations in identical food samples. This adaptation led to the development of a food-specific modeling factor, acknowledging that electrochemical responses could vary significantly across different food slurry matrices. These variations and the corresponding adjustments are thoroughly documented in the supporting

information (**Table S3**). Remarkably, this study represents the first instance of glyphosate being electrochemically detected in food samples with confirmation via LC-MS, diverging from previous methods that relied on testing biosensors with manually spiked food samples.[99] Moreover, the process for electrochemical detection of glyphosate in these food samples did not necessitate complex extraction procedures, streamlining the testing process. To analyze the robustness of each electrode, the electrodes were mechanically deformed around a 1 mm diameter rod (displayed in **Figure S12**), and the 2-point resistance of n=3 functionalized sensors was measured for both MoS_2- and $MoSe_2$-LIG (**Figure S13**). Over the course of 10 bending cycles, the resistance increased from 578 to 845 Ω and 588 to 787 Ω for MoS_2-LIG and $MoSe_2$-LIG, respectively. Note that the increase in resistance strongly correlated with the induced damage on the electrode surface caused by the probes as the surface noticeably deteriorated after each measurement. These results indicated that the electrodes maintained suitable conductivity without delamination and are sufficiently operable since the electrodes would not typically be exerted in such a manner while functioning in the food safety domain as compared to more aggressive applications (e.g., agriculture and wearables).

Table 1. Glyphosate in Food Samples

Food	Material	Adjusted Electrochemically Measured Concentration (ppm)	LC-MS Measured Concentration (ppm)	Recovery (%)
soybeans	MoS_2-LIG	1.3	1.6	81.3
canned pinto beans	MoS_2-LIG	4.7	5.5	85.5
soybeans	$MoSe_2$-LIG	1.9	1.6	119
canned pinto beans	$MoSe_2$-LIG	6.6	5.5	120

Conclusion

In conclusion, this work demonstrated the utility of MoS_2- and $MoSe_2$-LIG heterostructures in combination with the glyphosate biorecognition agent glycine oxidase for sensitive and specific determination of this herbicide. As such, this is the first work to harness the unique capabilities of both monodispersed MoS_2 and $MoSe_2$ suspensions deposited onto an LIG scaffold for the electrochemical detection of an herbicide. The use of MoS_2 and $MoSe_2$ circumvented the need for expensive catalytic materials like platinum, gold, or silver due to the electroactive and high surface area properties of the MoS_2/$MoSe_2$-LIG platform. Furthermore, the liquid phase exfoliation coupled with liquid cascade centrifugation are easy, time saving, economic, and large-scale methods. While liquid phase exfoliation is not entirely defect-free, it remains a practical and scalable method for producing 2D materials in which, by carefully optimizing the operating parameters, the extent of defects can be minimized. Conversely, the nanomaterial suspension was deposited using a tedious drop-coating procedure, which could be improved with an automated pipetting instrument. The developed MoS_2/$MoSe_2$-LIG biosensors maintained similar sensing properties of the noble metals but removed the added expense associated with noble metals. The biosensors detected glyphosate using differential pulse voltammetry over short time scales (~15 seconds) in a linear range from 10-90 μM with LODs of 4.0 and 6.1 μM, for the MoS_2-LIG and $MoSe_2$-LIG biosensors, respectively. The biosensors were further tested against common agricultural interferents including fungicides, insecticides, herbicides, food minerals, and the glyphosate metabolite (AMPA), which presented minimal interference. As final validation, the biosensors were tested in canned pinto bean and soybean slurries and verified with LC-MS using the Quick Polar Pesticides method.[98] The reported biosensors behaved similarly to other reported devices that detected glyphosate in food residues. In this work, however, chemical intensive

extraction procedures were not administered as was the case with the reported literature as well as the gold standard LC-MS method, which highlights the utility of the developed electrochemical devices.

The reported biosensor offers a viable platform for simple and rapid herbicide monitoring in food, generating broader implications regarding the utility of the $MoS_2/MoSe_2$-LIG platform. The ease-of-fabrication associated with $MoS_2/MoSe_2$ nanosheet liquid phase exfoliation via liquid cascade centrifugation and LIG produces a conductive base layer that can be rasterized into various designs while offering a rich amorphous structure necessary for nanomaterial and protein attachment that is essential in a multitude of other biosensing fields. The demonstrated sensing mechanism of reducing the enzymatic byproduct, H_2O_2, at negative potentials offers further utility to researchers who employ oxidase enzymes for biosensing purposes by circumventing higher oxidation potentials typically associated with oxidase biosensors. The $MoS_2/MoSe_2$ materials synthesized using a highly controllable method like liquid cascade centrifugation combined with LIG produced robust heterostructures conducive to sensing but could be further applied to a wider range of agrochemical (e.g., fertilizer ions, antibiotics, pesticides)[100] and biomedical (e.g., salmonella, dopamine, SARS-Cov-2)[101] monitoring as well as for energy systems using lignocellulose-based materials like cork and wood.[102]

Methods & Materials

1. Materials and Reagents

Sodium cholate (99%), molybdenum disulfide (99.9%), molybdenum diselenide (99.9%), 10X phosphate buffer saline (PBS) tablets dissolved in DI consisting of 2.7 mM KCl and 137 mM NaCl (pH 7.4), potassium hexacynoferrate (II) trihydrate (98.5%), potassium ferricyanide (99%), grade II glutaraldehyde (25%), flavin adenine dinucleotide (95%), glyphosate (99.9%), thiamethoxam

(99.9%), dicamba (99.9%), (aminomethyl)phosphonic acid (99%), carbendazim (99.9%), parathion (99.9%), iron (II) chloride (98%), zinc acetylacetonate hydrate (95%), glyphosate-2-^{13}C (99%) with M+1 mass shift, potassium chloride (99%), high molecular weight polyvinyl chloride (PVC) (K value of 69-71, 99.9%), tetrahydrofuran (THF) (anhydrous, 99.9%), 2-nitrophenyl octyl ether (NPOE) (99%), formic acid (95%), and ethyl-3-(3-dimethylaminopropyl) carbodiimide (99.9%)/*N*-hydroxysuccinimide (98%) (EDC/NHS) were purchased from Sigma Aldrich. All purchased pesticides were analytical standard. Methanol and KCl (99%) were purchased from Fisher Scientific. The glycine oxidase gene originates from *Bacillus subtilis* and gives rise to a 47 kDa protein. Glycine oxidase (40 μM) was prepared by the U.S. Naval Research Laboratory according to the reported protocols for other enzymes.[103,104] Glutaraldehyde and flavin adenine dinucleotide dilutions were prepared in 10X PBS pH 7.4 and 8.4, respectively. Glyphosate stock solutions (5 mM) were prepared in 10X PBS at pH 7.4. Kapton polyimide substrate (0.125 mm thick) was purchased from McMaster-Carr. Polyethylene terephthalate (PET) was purchased from Coveme (Kemafoil TSL W) with a thickness of 350 μm. Ag and Ag/AgCl pastes were purchased from Nagase ChemteX. All pesticides were prepared in 10X PBS. Unless otherwise specified, non-pesticide solutions were prepared in deionized water (18.2 mΩ cm). Soybeans and canned pinto beans were purchased from a local grocery store.

2. Synthesis of 2D-MoS_2 and 2D-$MoSe_2$ Nanosheets

The 2D-MoS_2 and 2D-$MoSe_2$ nanosheets were prepared via liquid phase exfoliation followed by cascade centrifugation. Exfoliation of MoS_2 powder (5 mg/mL) was carried out in a sodium cholate aqueous solution (1.5 mg/mL) with a Branson 250 sonifier operating at 50% of power for 30 minutes using an ice bath to reduce detrimental heating effects. The dispersions were left to decant overnight, resulting in samples where the supernatant contained MoS_2 flakes in liquid, with larger

crystallites settling at the bottom. This supernatant was then carefully separated from the sediment and subjected to centrifugation at 1.5 krpm for 90 minutes.[35,36,38,105] After this initial centrifugation, the supernatant was transferred to another vial for further centrifugation at 2 krpm for 90 minutes. This process was sequentially repeated at 3, 4, and 5 krpm to progressively refine the dispersion. The same procedure was applied to produce 2D-$MoSe_2$ nanosheets, ensuring a consistent approach to obtaining high-quality dispersions of these two-dimensional materials as investigated in a previous study, where batch-to-batch comparisons were made to ensure reproducible synthesis.[106,107] The sensing surface was tuned by applying 100 µL of each centrifuged suspension onto the LIG, where sensor responses were evaluated by performing voltametric scans in 1 mM H_2O_2. It was determined that sensors modified with the 1.5 krpm suspensions yielded the greatest response for both MoS_2/$MoSe_2$-LIG sensors. Therefore, the loading of the 1.5 krpm suspension was evaluated by varying the drop-coated volume on the sensing surface between 100 and 200 µL. These optimization studies are shown in **Figure S14.** Assessing the long-term biocompatibility of Mo-based nanosheet sensors requires a thorough understanding of their degradation and clearance pathways in biological environments. Mo-based nanosheets can break down into molybdenum ions and sulfur/selenium species, which are typically regarded as safe or have established metabolic pathways in the body. Additionally, clearance mechanisms like renal excretion may play a role in easily eliminating Mo-based nanosheets from the body. On what concerns the sodium cholate used as a surfactant, it is a bile salt commonly used in biomedical research and pharmaceutical formulations. It is also synthesized in the liver and follows well-known metabolic pathways in the body from which it is efficiently cleared.

3. LIG Fabrication and Modification

Kapton polyimide film was adhered to PET to improve rigidity. The Kapton was wiped with isopropyl alcohol before lasing. Once cleaned, the Kapton-PET sheet was taped to an aluminum plate and placed in the bed of the laser. The laser parameters were set to 15% speed, 7% power, 50% frequency, a 2 mm defocus, and a resolution of 1200 dots per inch based upon our previous studies that found these settings produced optimum electron transfer kinetics and minimized sheet resistance.[29] Electrode designs were prepared in CorelDRAW and then sent to the Epilog laser. Upon lasing, the laser converted the film into the porous LIG in the shape of the CorelDRAW file. All sensors were lased with a 3 mm working diameter. The electrical leads of the LIG, connecting to the working, reference, and counter electrodes, were coated with a layer of acrylic polish (passivation layer) to insulate the non-active parts. This ensures that only the designated active areas remain in contact with the solution throughout the sensing process. The electrical contact pads of the LIG, which were connected to the potentiostat using alligator clips, were coated with Ag paste to protect against abrasion and deterioration from repeated use of the clips. The LIG reference working area was coated with a Ag/AgCl paste to establish the reference electrode. Following the application of the Ag and Ag/AgCl pastes, the Kapton-PET sheet was cured on a hot plate at 100°C for 10 minutes. To complete the reference electrode, 1 µL of a salt-loaded PVC membrane was formulated and drop-cast over the Ag/AgCl reference using the following recipe: 32 mg PVC, 4 mg potassium chloride, 61.5 µL NPOE, and 1 mL of THF. To enhance the electrocatalytic nature of the LIG working electrodes, different volumes of 2D-MoS_2 and 2D-$MoSe_2$ dispersions were directly drop-cast onto the surface of the bare LIG working electrodes, which were simultaneously placed on a hot plate at 100°C to speed up drying.

4. Enzyme Functionalization onto LIG Electrodes

Glycine oxidase (40 μM in 10X PBS pH 7.4) and FAD (2 nM in 10X PBS pH 8.4) were mixed with varying concentrations of glutaraldehyde (0.01-0.25% in 10X PBS pH 7.4) in an equal volumetric ratio and then 4 μL of the resultant solution were pipetted onto the working electrode. This solution wetted the electrode for 5 minutes before excess solution was removed from the surface to maintain a thin film. For covalently linking enzyme to the sensors, EDC/NHS chemistry was employed with a solution of 0.4 M EDC and 0.1 M NHS was prepared in 0.1 M MES buffer (pH 6.0) and 5 μL were pipetted onto the working electrode and allowed to react for 90 minutes. Next these sensors were rinsed with MES buffer and then 4 μL of a mixture containing an equal volumetric ratio of enzyme (40 μM in 10X PBS pH 7.4) and FAD (2 nM in 10X PBS pH 8.4) were pipetted onto the electrode. As performed previously, this solution was allowed to wet the electrode for 5 minutes before excess solution was removed from the surface to maintain a thin film. Sensors were stored at 8° C prior to testing or in between tests to preserve the enzyme.

5. Material characterization

Raman spectroscopy measurements were performed using a Horiba XploRA Plus confocal Raman microscope with a 532 nm laser operating at 1.2 mW and a 50× objective (0.5 NA). The spectra were collected from 50 – 3600 cm^{-1} with a 600 grooves mm^{-1} grating. Eight Raman spectra were collected at 8 randomly selected locations, and each Raman spectrum was collected with a 30 s acquisition and 3 accumulations. Any spectral shift of the position of the peaks due to instrumental causes (generally a shift of all peaks of the same amount) has been corrected. All Raman peaks in each spectrum were fitted to a Lorentzian function in Igor Pro 6.37 to calculate the average I2D/IG ratio. SEMs were performed on an FEI Teneo field emission scanning electron microscope at an accelerating voltage of 5 kV and working distance of 7.7 mm using Optiplan mode. DLS was

performed on a Malvern Zetasizer Nano ZS using a wavelength of 635 nm and refractive index and adsorption of 5.2 and 1.1 for MoS_2 and 4.8 and 1.2 for $MoSe_2$. Samples were diluted [1:10 (v/v)] from the stock solutions, and the presented data was representative of the average of 3 measurements per sample.

6. Electrochemical Measurements

All electrochemical measurements were performed by a CHI 6281E electrochemical analyzer. Electrochemical characterization was performed using cyclic voltammetry (CV) at varying scan rates in 5 mM ferri/ferrocyanide with 0.1 M KCl as the supporting electrolyte. Differential pulse voltammetry (DPV) were ran in 10X PBS pH 7.4 between 0 and -0.7 V *vs* Ag/AgCl at an increment of 0.002 V, amplitude of 0.05 V, pulse width of 0.025 seconds, sampling width of 0.0125 seconds, pulse period of 0.05 seconds, and quiet time of 5 seconds. In the sensor test vial, glyphosate was mixed at 300 rpm for roughly 20 seconds before DPV measurements were performed. All experiments were performed at room temperature. Limits of detection (LOD) were calculated using the 3-sigma method as described in the Data and Statistical Analysis section below.

7. Food Sample Preparation

Canned pinto beans and soybeans were purchased from a local grocery store. Juice in the can was drained and the beans were collected. The following describes sample preparation for electrochemical sensing. First, 5 g of beans were weighed and then homogenized with a Hamilton Beach Coffee Grinder. The food sample was placed in a 50 mL falcon tube, and 5 mL of 10X PBS pH 7.4 was added to the tube. The sample was mixed on a G560 Vortex Genie 2 Mixer at 1250 rpm for 15 minutes to ensure adequate incorporation. Sensors were submerged into this mixture, and DPV scans were taken to obtain the electrochemical data. Food samples prepared for liquid chromatography-mass spectrometry (LC-MS) were prepared using a simplified Quick Polar

Pesticides (QuPPe) method.[98] In summary, 5 g of beans were ground and mixed with 10 mL of deionized water. Next, 15 ppm of the internal standard (glyphosate-2-^{13}C) was added. Note, the QuPPe calls for 80 ppb of the internal standard. However, given the limits of detection of the LC-MS instrument used, the internal standard concentration was increased to 15 ppm. This mixture rested for 30 minutes. Then, 10 mL of 1% (v/v) formic acid was added. The mixture rested for 30 minutes. Afterwards, the sample was placed on a Vortex Genie and mixed at 1250 rpm for 15 minutes. Immediately following, the mixture was placed in a -80º F freezer for 30 minutes. The mixture was centrifuged at 4500 rpm for 10 minutes. Supernatant liquid was collected and stored at -20º C until analyzed.

8. *Liquid Chromatography – Mass Spectrometry*

LC-MS was performed using an Agilent QTOF 6540. The instrument was run in negative ion mode. This method used an aqueous phase (0.1% formic acid) and solvent phase (0.1% formic acid in acetonitrile). A calibration curve was generated using increasing concentrations of glyphosate combined with the 15 ppm of the internal standard. The calibration curve was generated as the glyphosate peak area divided by the internal standard peak area to standardize the measurements. After the base peak chromatogram scan was complete, the chromatogram for the glyphosate peak values were extracted at a mass to charge ratio (m/z) of 168.0052. Similarly, the chromatogram of the glyphosate-2-^{13}C peak values were extracted at an m/z of 170.0063. The peaks were smoothed and the area under the curves were used for the calibration and predicted food concentrations (**Figure S9**).

9. *Data and Statistical Analysis*

The raw data from the DPV scans were used in the calibration model. Raw data was normalized by adjusting each DPV scan to a standard baseline in OriginPro. Current responses were taken as

the difference between the peak current near -0.15 V *vs* Ag/AgCl and the current found at the PBS baseline at the same potential location. The data was not fitted or filtered. Linear regression was performed in OriginPro, which yielded the linear sensitivity (s) and standard deviation of the y-intercept (σ). The σ was considered the noise, and the LOD was calculated using the 3σ method as described by LOD = 3σ/s. Sensor reproducibility and model calibration was determined as the average ± standard deviation for n = 4 sensors.

Acknowledgements

JCC gratefully acknowledges funding support for this work from the National Science Foundation under award number CMMI-2037026 as well as from the National Institute of Food and Agriculture, U.S. Department of Agriculture under award numbers 2021-67021-34457 and 2021-67011-35130. GN, PGG, and AF acknowledge funding by the European Union (NextGeneration EU) through the MUR-PNRR projects SAMOTHRACE (No. ECS00000022) and PRIN FLASH-2D (B53D23004150006). ILM acknowledges the Office of Naval Research, the U.S. Naval Research Laboratory (NRL), the NRL Nanoscience Institute, and the National Institute of Food and Agriculture, U.S. Department of Agriculture, under Award #2020-67021-31254 for funding support. The authors wish to acknowledge the University of Messina, Italy (UNIME) and Italian National Research Council - Institute for Chemical-Physical Processes of Messina (CNR-IPCF) for the synthesis of nanomaterials. The authors acknowledge the Iowa State University Chemical Instrumentation (CIF) for support and help with LC-MS experiments. All electron microscopy and related work were performed using instruments in the Sensitive Instrument Facility in Ames National Lab. The Ames National Laboratory is operated for the U.S. Department of Energy by Iowa State University under Contract No. DE-AC02-07CH11358. Additionally, the authors

acknowledge the University of Minnesota Characterization Facility for XPS. We acknowledge the use of BioRender to produce components in our figures.

References

(1) Maggi, F.; la Cecilia, D.; Tang, F. H. M.; McBratney, A. The Global Environmental Hazard of Glyphosate Use. *Science of The Total Environment* **2020**, *717*, 137167. https://doi.org/10.1016/J.SCITOTENV.2020.137167.

(2) van Bruggen, A. H. C.; He, M. M.; Shin, K.; Mai, V.; Jeong, K. C.; Finckh, M. R.; Morris, J. G. Environmental and Health Effects of the Herbicide Glyphosate. *Science of The Total Environment* **2018**, *616–617*, 255–268. https://doi.org/10.1016/J.SCITOTENV.2017.10.309.

(3) Benbrook, C. M. How Did the US EPA and IARC Reach Diametrically Opposed Conclusions on the Genotoxicity of Glyphosate-Based Herbicides? *Environ Sci Eur* **2019**, *31* (1), 1–16. https://doi.org/10.1186/S12302-018-0184-7.

(4) Székács, A.; Darvas, B. Re-Registration Challenges of Glyphosate in the European Union. *Front Environ Sci* **2018**, *6*, 78. https://doi.org/10.3389/FENVS.2018.00078.

(5) Gullickson, G. *Bayer to discontinue lawn and garden market glyphosate-based products starting in 2023 | Successful Farming*. Successful Farming. https://www.agriculture.com/news/business/bayer-to-discontinue-lawn-and-garden-market-glyphosate-based-products-starting-in-2023 (accessed 2022-09-19).

(6) Vicini, J. L.; Jensen, P. K.; Young, B. M.; Swarthout, J. T. Residues of Glyphosate in Food and Dietary Exposure. *Compr Rev Food Sci Food Saf* **2021**, *20* (5), 5226–5257. https://doi.org/10.1111/1541-4337.12822.

(7) Torretta, V.; Katsoyiannis, I. A.; Viotti, P.; Rada, E. C. Critical Review of the Effects of Glyphosate Exposure to the Environment and Humans through the Food Supply Chain. *Sustainability* **2018**, *10* (4), 950. https://doi.org/10.3390/SU10040950.

(8) Weston, M.; Geng, S.; Chandrawati, R.; Weston, M.; Geng, S.; Chandrawati, R. Food Sensors: Challenges and Opportunities. *Adv Mater Technol* **2021**, *6* (5), 2001242. https://doi.org/10.1002/ADMT.202001242.

(9) Valle, A. L.; Mello, F. C. C.; Alves-Balvedi, R. P.; Rodrigues, L. P.; Goulart, L. R. Glyphosate Detection: Methods, Needs and Challenges. *Environ Chem Lett* **2018**, *17* (1), 291–317. https://doi.org/10.1007/S10311-018-0789-5.

(10) Asano, K.; Sasaki, Y.; Minamiki, T.; Minami, T. Sensitive Detection of Glyphosate by a Water-Gated Organic Transistor. *ECS Trans* **2020**, *98* (12), 41–46. https://doi.org/10.1149/09812.0041ECST.

(11) Sasaki, Y.; Asano, K.; Minamiki, T.; Zhang, Z.; Takizawa, S.-Y.; Kubota, R.; Minami, T. A Water-Gated Organic Thin-Film Transistor for Glyphosate Detection: A Comparative Study with Fluorescence Sensing. *Chemistry – A European Journal* **2020**, *26* (64), 14525–14529. https://doi.org/10.1002/CHEM.202003529.

(12) Asano, K.; Didier, P.; Ohshiro, K.; Lobato-Dauzier, N.; Genot, A. J.; Minamiki, T.; Fujii, T.; Minami, T. Real-Time Detection of Glyphosate by a Water-Gated Organic Field-Effect Transistor with a Microfluidic Chamber. *Langmuir* **2021**, *37* (24), 7305–7311. https://doi.org/10.1021/ACS.LANGMUIR.1C00511.

(13) Gall, J. Le; Vasilijević, S.; Battaglini, N.; Mattana, G.; Noël, V.; Brayner, R.; Piro, B. Algae-Functionalized Hydrogel-Gated Organic Field-Effect Transistor. Application to the Detection of Herbicides. *Electrochim Acta* **2021**, *372*, 137881. https://doi.org/10.1016/J.ELECTACTA.2021.137881.

(14) Jiarui Yu; Jingyu Lin; Jianping Li. A Photoelectrochemical Sensor Based on an Acetylcholinesterase-CdS/ZnO-Modified Extended-Gate Field-Effect Transistor for Glyphosate Detection. *Analyst* **2021**, *146* (14), 4595–4604. https://doi.org/10.1039/D1AN00797A.
(15) Lowe, B. M.; Sun, K.; Zeimpekis, I.; Skylaris, C. K.; Green, N. G. Field-Effect Sensors – from PH Sensing to Biosensing: Sensitivity Enhancement Using Streptavidin–Biotin as a Model System. *Analyst* **2017**, *142* (22), 4173–4200. https://doi.org/10.1039/C7AN00455A.
(16) Qin, Y.; Wu, G.; Guo, Y.; Ke, D.; Yin, J.; Wang, D.; Fan, X.; Liu, Z.; Ruan, L.; Hu, Y. Engineered Glyphosate Oxidase Coupled to Spore-Based Chemiluminescence System for Glyphosate Detection. *Anal Chim Acta* **2020**, *1133*, 39–47. https://doi.org/10.1016/J.ACA.2020.07.077.
(17) Calabretta, M. M.; Zangheri, M.; Calabria, D.; Lopreside, A.; Montali, L.; Marchegiani, E.; Trozzi, I.; Guardigli, M.; Mirasoli, M.; Michelini, E. Paper-Based Immunosensors with Bio-Chemiluminescence Detection. *Sensors* **2021**, *21* (13), 4309. https://doi.org/10.3390/S21134309.
(18) Zouaoui, F.; Bourouina-Bacha, S.; Bourouina, M.; Abroa-Nemeir, I.; ben Halima, H.; Gallardo-Gonzalez, J.; el Alami El Hassani, N.; Alcacer, A.; Bausells, J.; Jaffrezic-Renault, N.; Zine, N.; Errachid, A. Electrochemical Impedance Spectroscopy Determination of Glyphosate Using a Molecularly Imprinted Chitosan. *Sens Actuators B Chem* **2020**, *309*, 127753. https://doi.org/10.1016/J.SNB.2020.127753.
(19) Zhao, P.; Yan, M.; Zhang, C.; Peng, R.; Ma, D.; Yu, J. Determination of Glyphosate in Foodstuff by One Novel Chemiluminescence-Molecular Imprinting Sensor. *Spectrochim Acta A Mol Biomol Spectrosc* **2011**, *78* (5), 1482–1486. https://doi.org/10.1016/J.SAA.2011.01.037.
(20) Piletsky, S.; Canfarotta, F.; Poma, A.; Bossi, A. M.; Piletsky, S. Molecularly Imprinted Polymers for Cell Recognition. *Trends Biotechnol* **2020**, *38* (4), 368–387. https://doi.org/10.1016/J.TIBTECH.2019.10.002.
(21) Gomes, N. O.; Paschoalin, R. T.; Bilatto, S.; Sorigotti, A. R.; Farinas, C. S.; Mattoso, L. H. C.; Machado, S. A. S.; Oliveira, O. N.; Raymundo-Pereira, P. A. Flexible, Bifunctional Sensing Platform Made with Biodegradable Mats for Detecting Glucose in Urine. *ACS Sustain Chem Eng* **2023**, *11* (6), 2209–2218. https://doi.org/10.1021/ACSSUSCHEMENG.2C05438.
(22) Teixeira, S. C.; Gomes, N. O.; Calegaro, M. L.; Machado, S. A. S.; de Oliveira, T. V.; de Fátima Ferreira Soares, N.; Raymundo-Pereira, P. A. Sustainable Plant-Wearable Sensors for on-Site, Rapid Decentralized Detection of Pesticides toward Precision Agriculture and Food Safety. *Biomaterials Advances* **2023**, *155*, 213676. https://doi.org/10.1016/J.BIOADV.2023.213676.
(23) Gomes, N. O.; Teixeira, S. C.; Calegaro, M. L.; Machado, S. A. S.; de Fátima Ferreira Soares, N.; de Oliveira, T. V.; Raymundo-Pereira, P. A. Flexible and Sustainable Printed Sensor Strips for On-Site, Fast Decentralized Self-Testing of Urinary Biomarkers Integrated with a Portable Wireless Analyzer. *Chemical Engineering Journal* **2023**, *472*, 144775. https://doi.org/10.1016/J.CEJ.2023.144775.
(24) Raymundo-Pereira, P. A.; Shimizu, F. M.; Coelho, D.; Piazzeta, M. H. O.; Gobbi, A. L.; Machado, S. A. S.; Oliveira, O. N. A Nanostructured Bifunctional Platform for Sensing of

Glucose Biomarker in Artificial Saliva: Synergy in Hybrid Pt/Au Surfaces. *Biosens Bioelectron* **2016**, *86*, 369–376. https://doi.org/10.1016/J.BIOS.2016.06.053.
(25) Paschoalin, R. T.; Gomes, N. O.; Almeida, G. F.; Bilatto, S.; Farinas, C. S.; Machado, S. A. S.; Mattoso, L. H. C.; Oliveira, O. N.; Raymundo-Pereira, P. A. Wearable Sensors Made with Solution-Blow Spinning Poly(Lactic Acid) for Non-Enzymatic Pesticide Detection in Agriculture and Food Safety. *Biosens Bioelectron* **2022**, *199*, 113875. https://doi.org/10.1016/J.BIOS.2021.113875.
(26) Pumera, M. Graphene in Biosensing. *Materials Today* **2011**, *14* (7–8), 308–315. https://doi.org/10.1016/S1369-7021(11)70160-2.
(27) Kucherenko, I. S.; Chen, B.; Johnson, Z.; Wilkins, A.; Sanborn, D.; Figueroa-Felix, N.; Mendivelso-Perez, D.; Smith, E. A.; Gomes, C.; Claussen, J. C. Laser-Induced Graphene Electrodes for Electrochemical Ion Sensing, Pesticide Monitoring, and Water Splitting. *Anal Bioanal Chem* **2021**, *413*, 6201–6212. https://doi.org/10.1007/S00216-021-03519-W.
(28) Liu, X.; Cheng, H.; Zhao, Y.; Wang, Y.; Li, F. Portable Electrochemical Biosensor Based on Laser-Induced Graphene and MnO2 Switch-Bridged DNA Signal Amplification for Sensitive Detection of Pesticide. *Biosens Bioelectron* **2022**, *199*, 113906. https://doi.org/10.1016/J.BIOS.2021.113906.
(29) Chen, B.; Johnson, Z. T.; Sanborn, D.; Hjort, R. G.; Garland, N. T.; Soares, R. R. A.; Belle, B. Van; Jared, N.; Li, J.; Jing, D.; Smith, E. A.; Gomes, C. L.; Claussen, J. C. Tuning the Structure, Conductivity, and Wettability of Laser-Induced Graphene for Multiplexed Open Microfluidic Environmental Biosensing and Energy Storage Devices. *ACS Nano* **2021**, *16*, 15–28. https://doi.org/10.1021/ACSNANO.1C04197.
(30) Wang, L.; Li, M.; Li, B.; Wang, M.; Zhao, H.; Zhao, F. Electrochemical Sensor Based on Laser-Induced Graphene for Carbendazim Detection in Water. *Foods* **2023**, *12* (12), 2277. https://doi.org/10.3390/FOODS12122277/S1.
(31) Johnson, Z. T.; Jared, N.; Peterson, J. K.; Li, J.; Smith, E. A.; Walper, S. A.; Hooe, S. L.; Breger, J. C.; Medintz, I. L.; Gomes, C.; Claussen, J. C. Enzymatic Laser-Induced Graphene Biosensor for Electrochemical Sensing of the Herbicide Glyphosate. *Global Challenges* **2022**, *6* (9), 2200057. https://doi.org/10.1002/GCH2.202200057.
(32) Zhuang, Z.; Huang, J.; Li, Y.; Zhou, L.; Mai, L. The Holy Grail in Platinum-Free Electrocatalytic Hydrogen Evolution: Molybdenum-Based Catalysts and Recent Advances. *ChemElectroChem* **2019**, *6* (14), 3570–3589. https://doi.org/10.1002/CELC.201900143.
(33) Singu, B. S.; Chitumalla, R. K.; Mandal, D.; Kim, Y.; Kim, G. H.; Chung, H. T.; Jang, J.; Kim, H. Development of Metal-Organic Framework-Derived NiMo-MoO3−x Porous Nanorod for Efficient Electrocatalytic Hydrogen Evolution Reactions. *Appl Catal B* **2023**, *328*, 122421. https://doi.org/10.1016/J.APCATB.2023.122421.
(34) Khan, R.; Radoi, A.; Rashid, S.; Hayat, A.; Vasilescu, A.; Andreescu, S. Two-Dimensional Nanostructures for Electrochemical Biosensor. *Sensors* **2021**, *21* (10), 3369. https://doi.org/10.3390/S21103369.
(35) Zribi, R.; Maalej, R.; Gillibert, R.; Donato, M. G.; Gucciardi, P. G.; Leonardi, S. G.; Neri, G. Simultaneous and Selective Determination of Dopamine and Tyrosine in the Presence of Uric Acid with 2D-MoS2 Nanosheets Modified Screen-Printed Carbon Electrodes. *FlatChem* **2020**, *24*, 100187. https://doi.org/10.1016/J.FLATC.2020.100187.
(36) Zribi, R.; Foti, A.; Donato, M. G.; Gucciardi, P. G.; Neri, G. Fabrication of a Novel Electrochemical Sensor Based on Carbon Cloth Matrix Functionalized with MoO3 and

2D-MoS2 Layers for Riboflavin Determination. *Sensors 2021, Vol. 21, Page 1371* **2021**, *21* (4), 1371. https://doi.org/10.3390/S21041371.

(37) Tongay, S.; Zhou, J.; Ataca, C.; Lo, K.; Matthews, T. S.; Li, J.; Grossman, J. C.; Wu, J. Thermally Driven Crossover from Indirect toward Direct Bandgap in 2D Semiconductors: MoSe2 versus MoS2. *Nano Lett* **2012**, *12* (11), 5576–5580. https://doi.org/10.1021/NL302584w.

(38) Zribi, R.; Maalej, R.; Messina, E.; Gillibert, R.; Donato, M. G.; Maragò, O. M.; Gucciardi, P. G.; Leonardi, S. G.; Neri, G. Exfoliated 2D-MoS2 Nanosheets on Carbon and Gold Screen Printed Electrodes for Enzyme-Free Electrochemical Sensing of Tyrosine. *Sens Actuators B Chem* **2020**, *303*, 127229. https://doi.org/10.1016/J.SNB.2019.127229.

(39) Murata, M.; Ivandini, T. A.; Shibata, M.; Nomura, S.; Fujishima, A.; Einaga, Y. Electrochemical Detection of Free Chlorine at Highly Boron-Doped Diamond Electrodes. *Journal of Electroanalytical Chemistry* **2008**, *612* (1), 29–36. https://doi.org/10.1016/J.JELECHEM.2007.09.006.

(40) Anindya, W.; Wahyuni, W. T.; Rafi, M.; Putra, B. R. Electrochemical Sensor Based on Graphene Oxide/PEDOT:PSS Composite Modified Glassy Carbon Electrode for Environmental Nitrite Detection. *Int J Electrochem Sci* **2023**, *18* (3), 100034. https://doi.org/10.1016/J.IJOES.2023.100034.

(41) Nasraoui, S.; Al-Hamry, A.; Teixeira, P. R.; Ameur, S.; Paterno, L. G.; Ben Ali, M.; Kanoun, O. Electrochemical Sensor for Nitrite Detection in Water Samples Using Flexible Laser-Induced Graphene Electrodes Functionalized by CNT Decorated by Au Nanoparticles. *Journal of Electroanalytical Chemistry* **2021**, *880*, 114893. https://doi.org/10.1016/J.JELECHEM.2020.114893.

(42) Bai, X.; Xu, Z.; Zhang, Q.; Li, S.; Dai, Y.; Cui, X.; Yoon, H. H.; Yao, L.; Jiang, H.; Du, M.; Zhang, Y.; Kauppinen, E. I.; Sun, Z. Molybdenum Disulfide/Double-Wall Carbon Nanotube Mixed-Dimensional Heterostructures. *Adv Mater Interfaces* **2022**, *9* (13), 2200193. https://doi.org/10.1002/ADMI.202200193.

(43) Subramanian, S.; Xu, K.; Wang, Y.; Moser, S.; Simonson, N. A.; Deng, D.; Crespi, V. H.; Fullerton-Shirey, S. K.; Robinson, J. A. Tuning Transport across MoS2/Graphene Interfaces via as-Grown Lateral Heterostructures. *NPJ 2D Mater Appl* **2020**, *4* (1), 9. https://doi.org/10.1038/s41699-020-0144-0.

(44) Wenelska, K.; Adam, V.; Thauer, E.; Singer, L.; Klingeler, R.; Chen, X.; Mijowska, E. Fabrication of 3D Graphene/MoS2 Spherical Heterostructure as Anode Material in Li-Ion Battery. *Front Energy Res* **2022**, *10*, 960786. https://doi.org/10.3389/FENRG.2022.960786.

(45) Pham, T.; Ramnani, P.; Villarreal, C. C.; Lopez, J.; Das, P.; Lee, I.; Neupane, M. R.; Rheem, Y.; Mulchandani, A. MoS2-Graphene Heterostructures as Efficient Organic Compounds Sensing 2D Materials. *Carbon N Y* **2019**, *142*, 504–512. https://doi.org/10.1016/J.CARBON.2018.10.079.

(46) Xu, L.; Huang, W. Q.; Hu, W.; Yang, K.; Zhou, B. X.; Pan, A.; Huang, G. F. Two-Dimensional MoS2-Graphene-Based Multilayer van Der Waals Heterostructures: Enhanced Charge Transfer and Optical Absorption, and Electric-Field Tunable Dirac Point and Band Gap. *Chemistry of Materials* **2017**, *29* (13), 5504–5512. https://doi.org/10.1021/ACS.CHEMMATER.7B00281.

(47) Hong, H. S.; Phuong, N. H.; Huong, N. T.; Nam, N. H.; Hue, N. T. Highly Sensitive and Low Detection Limit of Resistive NO2 Gas Sensor Based on a MoS2/Graphene Two-

Dimensional Heterostructures. *Appl Surf Sci* **2019**, *492*, 449–454. https://doi.org/10.1016/J.APSUSC.2019.06.230.
(48) Enebral-Romero, E.; Gutiérrez-Gálvez, L.; Del Caño, R.; Sulleiro, M. V.; Naranjo, A.; Gómez, I. J.; Pariente, F.; Pérez, E. M.; García-Mendiola, T.; Lorenzo, E. Pathogen Sensing Device Based on 2D MoS2/Graphene Heterostructure. *Sens Actuators B Chem* **2023**, *392*, 134105. https://doi.org/10.1016/J.SNB.2023.134105.
(49) Lee, C. S.; Kim, T. H. Large-Scale Preparation of MoS2/Graphene Composites for Electrochemical Detection of Morin. *ACS Appl Nano Mater* **2021**, *4* (7), 6668–6677. https://doi.org/10.1021/ACSANM.1C00622.
(50) Govindasamy, M.; Chen, S. M.; Mani, V.; Akilarasan, M.; Kogularasu, S.; Subramani, B. Nanocomposites Composed of Layered Molybdenum Disulfide and Graphene for Highly Sensitive Amperometric Determination of Methyl Parathion. *Microchimica Acta* **2017**, *184* (3), 725–733. https://doi.org/10.1007/S00604-016-2062-6.
(51) Zribi, R.; Foti, A.; Donato, M. G.; Gucciardi, P. G.; Neri, G. Electrochemical and Sensing Properties of 2D-MoS2 Nanosheets Produced via Liquid Cascade Centrifugation. *Electrochim Acta* **2022**, *436*, 141433. https://doi.org/10.1016/J.ELECTACTA.2022.141433.
(52) Gholamvand, Z.; McAteer, D.; Harvey, A.; Backes, C.; Coleman, J. N. Electrochemical Applications of Two-Dimensional Nanosheets: The Effect of Nanosheet Length and Thickness. *Chemistry of Materials* **2016**, *28* (8), 2641–2651. https://doi.org/10.1021/ACS.CHEMMATER.6B00009.
(53) Smith, R. J.; King, P. J.; Lotya, M.; Wirtz, C.; Khan, U.; De, S.; O'Neill, A.; Duesberg, G. S.; Grunlan, J. C.; Moriarty, G.; Chen, J.; Wang, J.; Minett, A. I.; Nicolosi, V.; Coleman, J. N. Large-Scale Exfoliation of Inorganic Layered Compounds in Aqueous Surfactant Solutions. *Advanced Materials* **2011**, *23* (34), 3944–3948. https://doi.org/10.1002/ADMA.201102584.
(54) Wang, Y. H.; Huang, K. J.; Wu, X. Recent Advances in Transition-Metal Dichalcogenides Based Electrochemical Biosensors: A Review. *Biosens Bioelectron* **2017**, *97*, 305–316. https://doi.org/10.1016/J.BIOS.2017.06.011.
(55) Hägele, F. *Glyphosate in Fruits and Vegetables – as Present as in the Media?* https://www.cvuas.de/pesticides/beitrag_en.asp?subid=1&Thema_ID=5&ID=3187&lang=EN&Pdf=No (accessed 2023-07-24).
(56) Lin, J.; Peng, Z.; Liu, Y.; Ruiz-Zepeda, F.; Ye, R.; Samuel, E. L. G.; Yacaman, M. J.; Yakobson, B. I.; Tour, J. M. Laser-Induced Porous Graphene Films from Commercial Polymers. *Nat Commun* **2014**, *5*, 5714. https://doi.org/10.1038/ncomms6714.
(57) Lingenfelter, P.; Bartoszewicz, B.; Migdalski, J.; Sokalski, T.; Bućko, M. M.; Filipek, R.; Lewenstam, A. Reference Electrodes with Polymer-Based Membranes—Comprehensive Performance Characteristics. *Membranes (Basel)* **2019**, *9* (12). https://doi.org/10.3390/membranes9120161.
(58) Pedotti, M.; Rosini, E.; Molla, G.; Moschetti, T.; Savino, C.; Vallone, B.; Pollegioni, L. Glyphosate Resistance by Engineering the Flavoenzyme Glycine Oxidase. *J Biol Chem* **2009**, *284* (52), 36415. https://doi.org/10.1074/JBC.M109.051631.
(59) Zribi, R.; Neri, G. Mo-Based Layered Nanostructures for the Electrochemical Sensing of Biomolecules. *Sensors* **2020**, *20* (18), 5404. https://doi.org/10.3390/S20185404.

(60) Shu, Y.; Zhang, W.; Cai, H.; Yang, Y.; Yu, X.; Gao, Q. Expanding the Interlayers of Molybdenum Disulfide toward the Highly Sensitive Sensing of Hydrogen Peroxide. *Nanoscale* **2019**, *11* (14), 6644–6653. https://doi.org/10.1039/C9NR00333A.
(61) Hu, J.; Zhang, C.; Li, X.; Du, X. An Electrochemical Sensor Based on Chalcogenide Molybdenum Disulfide-Gold-Silver Nanocomposite for Detection of Hydrogen Peroxide Released by Cancer Cells. *Sensors* **2020**, *20* (23), 6817. https://doi.org/10.3390/S20236817.
(62) Ramaraj, S.; Sakthivel, M.; Chen, S. M.; Lou, B. S.; Ho, K. C. Defect and Additional Active Sites on the Basal Plane of Manganese-Doped Molybdenum Diselenide for Effective Enzyme Immobilization: In Vitro and in Vivo Real-Time Analyses of Hydrogen Peroxide Sensing. *ACS Appl Mater Interfaces* **2019**, *11* (8), 7862–7871. https://doi.org/10.1021/ACSAMI.8B22389.
(63) Omrani, Z.; Pourmadadi, M.; Yazdian, F.; Rashedi, H. Preparation and Characterization of PH-Sensitive Chitosan/Starch/MoS2 Nanocomposite for Control Release of Curcumin Macromolecules Drug Delivery; Application in the Breast Cancer Treatment. *Int J Biol Macromol* **2023**, *250*, 125897. https://doi.org/10.1016/J.IJBIOMAC.2023.125897.
(64) Wu, J.; Ciucci, F.; Kim, J. K. Molybdenum Disulfide Based Nanomaterials for Rechargeable Batteries. *Chemistry – A European Journal* **2020**, *26* (29), 6296–6319. https://doi.org/10.1002/CHEM.201905524.
(65) Backes, C.; Szydłowska, B. M.; Harvey, A.; Yuan, S.; Vega-Mayoral, V.; Davies, B. R.; Zhao, P. L.; Hanlon, D.; Santos, E. J. G.; Katsnelson, M. I.; Blau, W. J.; Gadermaier, C.; Coleman, J. N. Production of Highly Monolayer Enriched Dispersions of Liquid-Exfoliated Nanosheets by Liquid Cascade Centrifugation. *ACS Nano* **2016**, *10* (1), 1589–1601. https://doi.org/10.1021/ACSNANO.5B07228.
(66) Chen, J. M.; Wang, C. S. Second Order Raman Spectrum of MoS2. *Solid State Commun* **1974**, *14* (9), 857–860. https://doi.org/10.1016/0038-1098(74)90150-1.
(67) Windom, B. C.; Sawyer, W. G.; Hahn, D. W. A Raman Spectroscopic Study of MoS 2 and MoO 3: Applications to Tribological Systems. *Tribol Lett* **2011**, *42* (3), 301–310. https://doi.org/10.1007/S11249-011-9774-x.
(68) Zhang, X.; Qiao, X. F.; Shi, W.; Wu, J. Bin; Jiang, D. S.; Tan, P. H. Phonon and Raman Scattering of Two-Dimensional Transition Metal Dichalcogenides from Monolayer, Multilayer to Bulk Material. *Chem Soc Rev* **2015**, *44* (9), 2757–2785. https://doi.org/10.1039/C4CS00282B.
(69) Sharma, P.; Thakur, D.; Kumar, D. Novel Enzymatic Biosensor Utilizing a MoS2/MoO3 Nanohybrid for the Electrochemical Detection of Xanthine in Fish Meat. *ACS Omega* **2023**, *8*, 31962–31971. https://doi.org/10.1021/ACSOMEGA.3C03776.
(70) Arya Nair, J. S.; Saisree, S.; Aswathi, R.; Sandhya, K. Y. Ultra-Selective and Real-Time Detection of Dopamine Using Molybdenum Disulphide Decorated Graphene-Based Electrochemical Biosensor. *Sens Actuators B Chem* **2022**, *354*, 131254. https://doi.org/10.1016/J.SNB.2021.131254.
(71) Yao, Z.; Yu, C.; Dai, H.; Zhou, J.; Liu, X.; Sun, G. Hybrid Fibers Assembled from MoSe2/Graphene Heterostructures Endow Improved Supercapacitive Performance. *Carbon N Y* **2022**, *187*, 165–172. https://doi.org/10.1016/J.CARBON.2021.11.009.
(72) Liu, Z.; Zhang, Y.; Zhao, H.; Li, N.; Du, Y. Constructing Monodispersed MoSe2 Anchored on Graphene: A Superior Nanomaterial for Sodium Storage. *Sci China Mater* **2017**, *60*, 167–177. https://doi.org/10.1007/s40843-016-5133-2.

(73) Huang, Y.; Wang, Z.; Guan, M.; Wu, F.; Chen, R. Toward Rapid-Charging Sodium-Ion Batteries Using Hybrid-Phase Molybdenum Sulfide Selenide-Based Anodes. *Advanced Materials* **2020**, *32* (40), 2003534. https://doi.org/10.1002/ADMA.202003534.
(74) Ferrari, A. C.; Meyer, J. C.; Scardaci, V.; Casiraghi, C.; Lazzeri, M.; Mauri, F.; Piscanec, S.; Jiang, D.; Novoselov, K. S.; Roth, S.; Geim, A. K. Raman Spectrum of Graphene and Graphene Layers. *Phys Rev Lett* **2006**, *97* (18), 187401. https://doi.org/10.1103/PhysRevLett.97.187401.
(75) Nguyen, V. T.; Le, H. D.; Nguyen, V. C.; Ngo, T. T. T.; Le, D. Q.; Nguyen, X. N.; Phan, N. M. Synthesis of Multi-Layer Graphene Films on Copper Tape by Atmospheric Pressure Chemical Vapor Deposition Method. *Advances in Natural Sciences: Nanoscience and Nanotechnology* **2013**, *4* (3), 35012. https://doi.org/10.1088/2043-6262/4/3/035012.
(76) Lin, Q.; Dong, X.; Wang, Y.; Zheng, N.; Zhao, Y.; Xu, W.; Ding, T. Molybdenum Disulfide with Enlarged Interlayer Spacing Decorated on Reduced Graphene Oxide for Efficient Electrocatalytic Hydrogen Evolution. *J Mater Sci* **2020**, *55* (15), 6637–6647. https://doi.org/10.1007/S10853-020-04478-W.
(77) Romanov, R. I.; Slavich, A. S.; Kozodaev, M. G.; Myakota, D. I.; Lebedinskii, Y. Y.; Novikov, S. M.; Markeev, A. M. Band Alignment in As-Transferred and Annealed Graphene/MoS2 Heterostructures. *physica status solidi (RRL) – Rapid Research Letters* **2020**, *14* (2), 1900406. https://doi.org/10.1002/PSSR.201900406.
(78) Yu, C.; Xu, H.; Sun, Y.; Zhao, X.; Hui, Z.; Gong, Y.; Chen, R.; Chen, Q.; Zhou, J.; Sun, G.; Huang, W. The Incorporation of Expanded 1T-Enriched MoS2 Boosts Hybrid Fiber Improved Charge Storage Capability. *Carbon N Y* **2020**, *170*, 543–549. https://doi.org/10.1016/J.CARBON.2020.08.017.
(79) Qu, Y.; Medina, H.; Wang, S.-W.; Wang, Y.-C.; Chen, C.-W.; Su, T.-Y.; Manikandan, A.; Wang, K.; Shih, Y.-C.; Chang, J.-W.; Kuo, H.-C.; Lee, C.-Y.; Lu, S.-Y.; Shen, G.; Wang, Z. M.; Chueh, Y.-L.; Qu, Y. D.; Wang, Z. M.; Medina, H.; Wang, Y.; Chen, C.; Su, T.; Manikandan, A.; Wang, K.; Shih, Y.; Lee, C.; Chueh, Y.; Wang, S.; Kuo, H.; Chang, J.; Lu, S.; Shen, G. Wafer Scale Phase-Engineered 1T- and 2H-MoSe2/Mo Core–Shell 3D-Hierarchical Nanostructures toward Efficient Electrocatalytic Hydrogen Evolution Reaction. *Advanced Materials* **2016**, *28* (44), 9831–9838. https://doi.org/10.1002/ADMA.201602697.
(80) Yi, M.; Zhang, C. The Synthesis of Two-Dimensional MoS 2 Nanosheets with Enhanced Tribological Properties as Oil Additives. *RSC Adv* **2018**, *8* (17), 9564–9573. https://doi.org/10.1039/C7RA12897E.
(81) Rathi, K.; Pal, K.; Rathi, K.; Pal, K. Fabrication of MoSe2–Graphene Hybrid Nanoflakes for Toxic Gas Sensor with Tunable Sensitivity. *Adv Mater Interfaces* **2020**, *7* (12), 2000140. https://doi.org/10.1002/ADMI.202000140.
(82) Ling, M.; Jiang, B.; Cao, X.; Wu, T.; Cheng, Y.; Zeng, P.; Zhang, L.; Cheong, W. C. M.; Wu, K.; Huang, A.; Wei, X. Phase-Controllable Synthesis of Multifunctional 1T-MoSe2 Nanostructures: Applications in Lithium-Ion Batteries, Electrocatalytic Hydrogen Evolution, and the Hydrogenation Reaction. *ChemElectroChem* **2021**, *8* (21), 4148–4155. https://doi.org/10.1002/CELC.202101146.
(83) Zambrano-Intriago, L. A.; Amorim, C. G.; Araújo, A. N.; Gritsok, D.; Rodríguez-Díaz, J. M.; Montenegro, M. C. B. S. M. Development of an Inexpensive and Rapidly Preparable Enzymatic Pencil Graphite Biosensor for Monitoring of Glyphosate in Waters. *Science of*

The Total Environment **2023**, *855*, 158865. https://doi.org/10.1016/J.SCITOTENV.2022.158865.
(84) Ferrari, A. G. M.; Foster, C. W.; Kelly, P. J.; Brownson, D. A. C.; Banks, C. E. Determination of the Electrochemical Area of Screen-Printed Electrochemical Sensing Platforms. *Biosensors 2018, Vol. 8, Page 53* **2018**, *8* (2), 53. https://doi.org/10.3390/BIOS8020053.
(85) Urbanová, V.; Bakandritsos, A.; Jakubec, P.; Szambó, T.; Zbořil, R. A Facile Graphene Oxide Based Sensor for Electrochemical Detection of Neonicotinoids. *Biosens Bioelectron* **2017**, *89*, 532–537. https://doi.org/10.1016/j.bios.2016.03.039.
(86) Hjort, R. G.; Pola, C. C.; Soares, R. R. A.; Opare-Addo, J.; Smith, E. A.; Claussen, J. C.; Gomes, C. L. Laser-Induced Graphene Decorated with Platinum Nanoparticles for Electrochemical Analysis of Saliva. *ACS Appl Nano Mater* **2023**, *6*, 20801–20811. https://doi.org/10.1021/ACSANM.3C03786.
(87) Migneault, I.; Dartiguenave, C.; Bertrand, M. J.; Waldron, K. C. Glutaraldehyde: Behavior in Aqueous Solution, Reaction with Proteins, and Application to Enzyme Crosslinking. *Biotechniques* **2004**, *37* (5), 790–802. https://doi.org/10.2144/04375RV01.
(88) Nguyen, H. H.; Lee, S. H.; Lee, U. J.; Fermin, C. D.; Kim, M. Immobilized Enzymes in Biosensor Applications. *Materials* **2019**, *12* (1), 121. https://doi.org/10.3390/MA12010121.
(89) Hoyos-Arbeláez, J.; Vázquez, M.; Contreras-Calderón, J. Electrochemical Methods as a Tool for Determining the Antioxidant Capacity of Food and Beverages: A Review. *Food Chem* **2017**, *221*, 1371–1381. https://doi.org/10.1016/j.foodchem.2016.11.017.
(90) Jared, N. M.; Johnson, Z. T.; Pola, C. C.; Bez, K. K.; Bez, K.; Hooe, S. L.; Breger, J. C.; Smith, E. A.; Medintz, I. L.; Neihart, N. M.; Claussen, J. C. Biomimetic Laser-Induced Graphene Fern Leaf and Enzymatic Biosensor for Pesticide Spray Collection and Monitoring. *Nanoscale Horiz* **2024**. https://doi.org/10.1039/D4NH00010B.
(91) Wang, Q.; Liu, Y.; Campillo-Brocal, J. C.; Jiménez-Quero, A.; Crespo, G. A.; Cuartero, M. Electrochemical Biosensor for Glycine Detection in Biological Fluids. *Biosens Bioelectron* **2021**, *182*, 113154. https://doi.org/10.1016/J.BIOS.2021.113154.
(92) Elgrishi, N.; Rountree, K. J.; McCarthy, B. D.; Rountree, E. S.; Eisenhart, T. T.; Dempsey, J. L. A Practical Beginner's Guide to Cyclic Voltammetry. *J Chem Educ* **2018**, *95* (2), 197–206. https://doi.org/10.1021/acs.jchemed.7b00361.
(93) Garcia, E. M.; Cordero, P. A.; Kazemeini, S.; Murillo-Soto, A.; Gonzalez, K. A.; McClement, A.; Rusinek, C. A. Platinum and Palladium Nanoparticles on Boron-Doped Diamond for the Electrochemical Detection of Hydrogen Peroxide: A Comparison Study. *Anal Bioanal Chem* **2023**, *415* (23), 5781–5795. https://doi.org/10.1007/S00216-023-04859-5.
(94) Rubenwolf, S.; Kerzenmacher, S.; Zengerle, R.; Von Stetten, F. Strategies to Extend the Lifetime of Bioelectrochemical Enzyme Electrodes for Biosensing and Biofuel Cell Applications. *Appl Microbiol Biotechnol* **2011**, *89* (5), 1315–1322. https://doi.org/10.1007/S00253-010-3073-6.
(95) Weltz, J. S.; Kienle, D. F.; Schwartz, D. K.; Kaar, J. L. Reduced Enzyme Dynamics upon Multipoint Covalent Immobilization Leads to Stability-Activity Trade-Off. *J Am Chem Soc* **2020**, *142* (7), 3463–3471. https://doi.org/10.1021/JACS.9B11707.

(96) Craddock, H. A.; Huang, D.; Turner, P. C.; Quirós-Alcalá, L.; Payne-Sturges, D. C. Trends in Neonicotinoid Pesticide Residues in Food and Water in the United States, 1999-2015. *Environ Health* **2019**, *18* (1), 1–16. https://doi.org/10.1186/S12940-018-0441-7.
(97) Meyers, S. L.; Arana, J.; Woolam, B. C.; Vargas, N.; Rodriguez, L.; Cardona, L. Dicamba Residue Persistence in Processing Tomato. *Weed Sci* **2022**, *70* (5), 603–609. https://doi.org/10.1017/WSC.2022.46.
(98) Shimelis, O. I.; Marsala, T.; Ross, M. J. *Simplified LC-MS/MS Method for Glyphosate, AMPA, and Glufosinate in Oat-Based Cereals*. https://www.sigmaaldrich.com/US/en/technical-documents/technical-article/food-and-beverage-testing-and-manufacturing/chemical-analysis-for-food-and-beverage/simplified-lc-ms-ms-method-for-glyphosate-ampa-and-glufosinate-in-oat-based-cereals?gclid=EAIaIQobChMIpLPG4OmqgAMVFymzAB2-xAwAEAAYASAAEgLGpfD_BwE&gclsrc=aw.ds (accessed 2023-07-24).
(99) Zambrano-Intriago, L. A.; Amorim, C. G.; Rodríguez-Díaz, J. M.; Araújo, A. N.; Montenegro, M. C. B. S. M. Challenges in the Design of Electrochemical Sensor for Glyphosate-Based on New Materials and Biological Recognition. *Science of The Total Environment* **2021**, *793*, 148496. https://doi.org/10.1016/J.SCITOTENV.2021.148496.
(100) Wanjari, V. P.; Reddy, A. S.; Duttagupta, S. P.; Singh, S. P. Laser-Induced Graphene-Based Electrochemical Biosensors for Environmental Applications: A Perspective. *Environmental Science and Pollution Research* **2022**, *30* (15), 42643–42657. https://doi.org/10.1007/S11356-022-21035-X.
(101) Liu, J.; Ji, H.; Lv, X.; Zeng, C.; Li, H.; Li, F.; Qu, B.; Cui, F.; Zhou, Q. Laser-Induced Graphene (LIG)-Driven Medical Sensors for Health Monitoring and Diseases Diagnosis. *Microchimica Acta* **2022**, *189* (2), 1–14. https://doi.org/10.1007/S00604-021-05157-6.
(102) Le, T. S. D.; Phan, H. P.; Kwon, S.; Park, S.; Jung, Y.; Min, J.; Chun, B. J.; Yoon, H.; Ko, S. H.; Kim, S. W.; Kim, Y. J. Recent Advances in Laser-Induced Graphene: Mechanism, Fabrication, Properties, and Applications in Flexible Electronics. *Adv Funct Mater* **2022**, *32* (48), 2205158. https://doi.org/10.1002/ADFM.202205158.
(103) Breger, J. C.; Oh, E.; Susumu, K.; Klein, W. P.; Walper, S. A.; Ancona, M. G.; Medintz, I. L. Nanoparticle Size Influences Localized Enzymatic Enhancement - A Case Study with Phosphotriesterase. *Bioconjug Chem* **2019**, *30* (7), 2060–2074. https://doi.org/10.1021/ACS.BIOCONJCHEM.9B00362.
(104) Vranish, J. N.; Ancona, M. G.; Oh, E.; Susumu, K.; Lasarte Aragonés, G.; Breger, J. C.; Walper, S. A.; Medintz, I. L. Enhancing Coupled Enzymatic Activity by Colocalization on Nanoparticle Surfaces: Kinetic Evidence for Directed Channeling of Intermediates. *ACS Nano* **2018**, *12* (8), 7911–7926. https://doi.org/10.1021/ACSNANO.8B02334.
(105) Backes, C.; Smith, R. J.; McEvoy, N.; Berner, N. C.; McCloskey, D.; Nerl, H. C.; O'Neill, A.; King, P. J.; Higgins, T.; Hanlon, D.; Scheuschner, N.; Maultzsch, J.; Houben, L.; Duesberg, G. S.; Donegan, J. F.; Nicolosi, V.; Coleman, J. N. Edge and Confinement Effects Allow in Situ Measurement of Size and Thickness of Liquid-Exfoliated Nanosheets. *Nature Communications 2014 5:1* **2014**, *5* (1), 1–10. https://doi.org/10.1038/ncomms5576.
(106) Abid, K.; Foti, A.; Khaskhoussi, A.; Celesti, C.; D'Andrea, C.; Polykretis, P.; Matteini, P.; Iannazzo, D.; Maalej, R.; Gucciardi, P. G.; Neri, G. A Study of Screen-Printed Electrodes Modified with MoSe2 and AuNPs-MoSe2 Nanosheets for Dopamine Sensing.

Electrochim Acta **2024**, *475*, 143371. https://doi.org/10.1016/J.ELECTACTA.2023.143371.

(107) Sharma, R.; Dawar, A.; Ojha, S.; Laishram, R.; Sathe, V. G.; Srivastava, R.; Sinha, O. P. A Thrifty Liquid-Phase Exfoliation (LPE) of MoSe2 and WSe2 Nanosheets as Channel Materials for FET Application. *J Electron Mater* **2023**, *52* (4), 2819–2830. https://doi.org/10.1007/S11664-023-10245-9.

TOC Figure (55 mm x 50 mm)